HyperTRIBE mapping of the RNA m^{6}A demethylase ALKBH9 binding sites in bamboo reveals its role in plant defense

Huihui Wang[1,†], Huiyuan Wang[1,†], Yue Jia[2], Tuhe Li[1], Siyu Yang[2], Yandong Jin[1], Zaofa Zhong[2], Wenting Bai[2], Huakun Zheng[3], Liangzhen Zhao[2], Chentao Lin[2], Anireddy S. N. Reddy[4], Hangxiao Zhang[2], Lianfeng Gu[2*]

[1] College of Forestry, Fujian Agriculture and Forestry University, Fuzhou 350002, China.
[2] Fujian Provincial Key Laboratory of Haixia Applied Plant Systems Biology, Basic Forestry and Proteomics Research Center, Haixia Institute of Science and Technology, Fujian Agriculture and Forestry University, Fuzhou 350002, China.
[3] National Engineering Research Center of JUNCAO Technology, Fujian Agriculture and Forestry University, Fuzhou 350002, China
[4] Department of Biology and Program in Cell and Molecular Biology, Colorado State University, Fort Collins, Colorado, USA

[*]Corresponding author: lfgu@fafu.edu.cn (L.G.)

[†]These authors contributed equally.

Short title: PheALKBH9 regulates defense responses in plants

The author responsible for distribution of materials integral to the findings presented in this article in accordance with the policy described in the Instructions for Authors (https://academic.oup.com/plphys/pages/General-Instructions) is Lianfeng Gu.

Abstract

RNA demethylation plays an important role in diverse biological processes. Intriguingly, RNA demethylation has not been reported in bamboo, which is known for its rapid growth. PheALKBH9, an m^{6}A demethylase in bamboo, was stably transformed into rice and increased its susceptibility to rice blast disease. Heterologous expression of *PheALKBH9* reduced the overall m^{6}A modification levels in rice. Using HyperTRIBE (Targets of RNA-binding proteins Identified By Editing), we identified evolutionarily conserved PheALKBH9 target RNAs in both rice and Moso bamboo. Overexpression of PheALKBH9 led to higher protein expression and shorter poly(A) tails. Notably, PheALKBH9 directly bound to *CCR4-associated factor1* (*CAF1G*) and

Poly(A)-binding genes (*PABPC1* and *PABPC2*), potentially modulating poly(A) tail lengths. In addition, PheALKBH9 also bound to and removed m^6A modifications from *Perox4*, *JAZ7* and *METS2,* key players in plant immunity, suggesting that PheALKBH9 plays a role in plant disease resistance. In summary, our study unveils a previously unknown role of PheALKBH9-mediated m^6A demethylation in response to blast disease and provides insights into its mechanisms in monocotyledonous plants.

Introduction

Chemical modifications on RNA affect the processing and metabolism of RNA in various ways. To date, more than 160 RNA modifications have been discovered, among which RNA N^6-methyladenosine (m^6A) is the most prevalent one (Yue et al., 2015; Boccaletto et al., 2022). The m^6A modification is primarily controlled by m^6A methyltransferases ('writers'), binding proteins ('readers'), and demethylases ('erasers'), which respectively install, recognize, and remove m^6A modifications. In *Arabidopsis*, multiple protein complexes of m^6A writers have been identified, including MTA (homologous to METTL3), MTB (homologous to METTL14), FIP37 (homologous to WTAP), VIR (homologous to VIRMA), HAKAI, etc (Vespa et al., 2004; Zhong et al., 2008; Shen et al., 2016; Ruzicka et al., 2017).The inactivation of MTA hinders the development of plant embryos at the spherical stage, ultimately leading to embryonic death (Zhong et al., 2008). The homologue of mammalian methyltransferase METTL16, FIONA1, has been reported to participate in photomorphogenesis and floral transition (Wang et al., 2022; Xu et al., 2022). FIP37 in *Arabidopsis* interacts with MTA and negatively regulates the mRNA stability of several key genes, participating in maintaining the normal proliferation of stem meristems (Shen et al., 2016). Disruption of the *AtFIP37* in *Arabidopsis* results in endosperm and embryo development arrest (Vespa et al., 2004; Zhong et al., 2008). In rice, *OsFIP* and *OsMTA2* are also crucial for the development of male gametes, which affects rice pollen development and fertility (Zhang et al., 2019). These findings indicate an important role for m^6A writers in regulating embryonic development in plants.

The action of m^6A methyltransferases and demethylases makes m^6A methylation dynamic

and reversible (Shi et al., 2019). Demethylases in mammals represented by fat mass and obesity-associated protein, FTO, and ALKBH5 possess the ability to "erase" m^6A modifications (Jia et al., 2011; Zheng et al., 2013). Knocking out ALKBH9B results in hypersensitivity to abscisic acid (ABA) treatment during seed germination and early seedling development in *Arabidopsis* (Tang et al., 2022). Additionally, it has been reported that suppressing ALKBH9B expression in *Arabidopsis* reduces the accumulation of Alfalfa mosaic virus (AMV) by impairing the infectivity of the virus. This suggests that m^6A modification in plants may be used to regulate RNA virus replication in host organisms (Martinez-Perez et al., 2017). As m^6A deposition altered abundance and cleavage of transcripts involved in plant immunity, *mta* mutant and *ALKBH10B* overexpressing line enhanced their ability to resist bacterial and fungal pathogens in Arabidopsis (Prall et al., 2023). In addition, defect of *hakai* leads to constitutive overexpression of defense genes and enhanced resistance of Arabidopsis against biotrophic oomycete (*Hpa*) (Furci et al., 2024). m^6A reader MhYTP2 confers powdery mildew resistance in apple by regulating *MdMLO19* mRNA stability and antioxidant genes translation efficiency (Guo et al., 2022). Recently, researchers identified the mRNA m^6A demethylase OsALKBH9 in rice and demonstrated its function in male fertility regulation. Knockout of *OsALKBH9* caused defective tapetal programmed cell death (PCD) and excessive accumulation of microspores exine, which ultimately leads to male sterility (Tang et al., 2024). Apart from ALKBH9B, ALKBH10B also possesses a demethylation function in *Arabidopsis*. ALKBH10B regulates the flowering process by affecting mRNA stability via m^6A demethylation (Duan et al., 2017). Moreover, mutation of the m^6A demethylase SlALKBH2 in tomato results in increased m^6A levels in *SlDML2* mRNA and decreased mRNA abundance, leading to abnormal fruit maturation (Zhou et al., 2019). Interestingly, the heterologous expression of FTO in rice and potato can increase field yield and biomass by ~50% through regulating the chromatin architecture and transcription of genes in various metabolic pathways (Yu et al., 2021). However, the function of demethylases in the forest tree species remains unknown.

Both m^6A methyltransferases and demethylases are RNA-binding proteins (RBPs).

Deciphering their binding RNA will be crucial for understanding the functions. Currently, it can be achieved by ultraviolet cross-linking immunoprecipitation (CLIP) method and the developed HyperTRIBE method (Targets of RNA-binding proteins Identified By Editing, TRIBE) (Ramanathan et al., 2019). In HyperTRIBE, an RBP-fused adenosine deaminase acting on RNA (ADAR) can convert adenosine to inosine near the binding sites (Xu et al., 2018). Compared with the traditional CLIP-seq method, HyperTRIBE is easy to operate and has a wide range of applications. For example, the target RNAs of the stress granule marker UBP1c protein have been successfully identified in Arabidopsis and rice using the HyperTRIBE method (Zhou et al., 2021). Researchers applied HyperTRIBE to identify the RNA bound by m^6A reader proteins ECT2 and ECT3 in Arabidopsis and found that they share most RNA targets (Arribas-Hernandez et al., 2021). What's more, the high-efficiency RNA editing ability of HyperTRIBE in plants is verified by using the interaction system of MCP-MS2 and AtGRP7 in rice and *Arabidopsis* protoplasts, respectively (Yin et al., 2023).

Research on m^6A methyltransferases, demethylases, and methylation reader proteins is mainly focused on model plants such as *Arabidopsis* and rice, leaving a blank slate for tree species. As one of the important tree species, *Phyllostachys edulis* has the characteristics of rapid growth, and it can grow as fast as one meter a day. In this study, we identified the m^6A RNA demethylase PheALKBH9 in Moso bamboo, which can reduce the level of m^6A modification. Overexpression of PheALKBH9 in rice leads to a more sensitive phenotype to rice blast disease. With the emerging HyperTRIBE method, we identified PheALKBH9 target RNAs in rice and Moso bamboo and found that some of the target RNAs are conserved. PheALKBH9 could regulate the poly(A) tail length (PAL) through binding to *OsCAF1G, PABPC1* and *PABPC2* in rice. In addition, PheALKBH9 also binds to and demethylates key genes such as *Perox4*, *OsJAZ7*, and *OsMETS2*, which are pivotal in the plant's response to blast disease. Our study reveals the functions of *PheALKBH9* in mRNA m^6A modification in Moso bamboo and rice, providing its mechanisms in responding to biotic stress in monocotyledonous plants.

Results

PheALKBH9 is involved in response to abiotic and biotic stresses in bamboo

Overexpression of the human RNA demethylase FTO in rice increases yield and biomass by approximately 50% (Yu et al., 2021). This suggests the potential of m^6A eraser in enhancing biomass. Identifying key methylation enzymes regulating biomass in plants could provide breeding strategies for crop improvement. Bamboo's high growth rate makes it an ideal material for studying rapid growth. Twelve ALKBH genes in *Phyllostachys edulis* **(**Supplementary **Table S1)** were classified into 8 subfamilies according to the evolutionary tree **(Figure 1A)**. In this study, *PheALKBH9* (*PH02Gene00238*) of Moso bamboo, which is evolutionarily closest to Arabidopsis m^6A RNA demethylase gene *AT2G17970* (*ALKBH9B*), was selected for functional investigation. Based on the previous transcriptome data (Vasupalli et al., 2021), we found that *PheALKBH9* was upregulated in response to PEG, NaCl, ABA, or salicylic acid (SA) treatment in Moso bamboo **(Figure 1B)**. We infected Moso bamboo leaves with Bamboo Mosaic Virus (BMV), a positive-sense single-stranded RNA virus. RT-qPCR results showed that *PheALKBH9* was down-regulated upon BaMV infection **(Figure 1C)**. The above results indicate that *PheALKBH9* may be involved in the response to both abiotic and biotic stresses in Moso bamboo. To determine the subcellular localization of PheALKBH9, we transiently expressed *$35S_{PRO}$:PheALKBH9-GFP* by agroinfiltration in tobacco leaves. Green fluorescence was detected in the cytoplasm, and we also observed some GFP signals in the nucleus **(Figure 1D)**. The results suggest that PheALKBH9 is mainly localized in the cytoplasm but may transfer into the nucleus under some conditions, which is consistent with the previous studies of AtALKBH9B in *Arabidopsis* (Martinez-Perez et al., 2017) and OsALKBH9 in rice (Tang et al., 2024).

Overexpression of PheALKBH9 reduces resistance to blast disease

In order to investigate the effect of *PheALKBH9* on plant growth, we constructed a *$35S_{PRO}$:PheALKBH9-GFP* vector and overexpressed it in Kitaake (*Oryza sativa* ssp *japonica*)

using Agrobacterium-mediated genetic transformation. Lines with high expression (lines 12 and 18) were selected for subsequent experiments **(**Supplementary **Figure S1A)**. *OE-PheALKBH9* exhibited no significant difference compared to the wild type (WT) from seedling to mature stages **(Figure 1E,** Supplementary **Figure S1B)**. Overexpression of *PheALKBH9* did not change the length, width, or aspect ratio of grain in rice **(Figure 1, F and G)**.

In rice, blast disease is one of the most serious problems, posing a major threat to rice production. Therefore, we inoculated WT and *OE-PheALKBH9* seedlings with *Magnaporthe oryzae* Guy11. The results showed that *OE-PheALKBH9* was more sensitive to rice blast **(Figure 1H)**. The lesion number of *OE-PheALKBH9* was higher than WT. DNA-based quantitative PCR with *M. oryzae Pot2* demonstrated that the relative fungal biomass on the leaves of *OE-PheALKBH9* was also higher **(Figure 1I)**. These results demonstrate that overexpression of *PheALKBH9* reduces the resistance of rice to blast disease. In addition to biotic stress, abiotic stress like salt stress also affects the growth and yield of rice. To validate the function of *PheALKBH9* on salt tolerance in rice, 3-week-old WT and *OE-PheALKBH9* were treated with 150 mM NaCl for 9 days. We found that the survival rate of WT rice was 60-70%, while the rate of *OE-PheALKBH9-12* and *OE-PheALKBH9-18* was 28% and 48% respectively. After high salt treatment, seedlings were transferred to recover in normal nutrient solution for 5 days. Compared to WT, more seedlings of *OE-PheALKBH9-12* and *OE-PheALKBH9-18* withered significantly. Especially all *OE-PheALKBH9-12* seedlings died without any revival **(**Supplementary **Figure S2)**, suggesting that overexpression of *PheALKBH9* reduces the resistance of rice to salt stress.

Overexpression of *PheALKBH9* reduced the overall level of m^{6}A modification

In order to confirm whether PheALKBH9 can regulate m^{6}A in plants, we used Nanopore direct RNA sequencing (DRS) on both *OE-PheALKBH9-12* and *OE-PheALKBH9-18* to detect m^{6}A modifications on mRNA **(**Supplementary **Table S2)**. We identified 6,012 and 5,919 genes with m^{6}A modification in WT and *OE-PheALKBH9* respectively, corresponding to 26,050 and 24,318 sites **(Figure 2, A and B)**, with an average of 4-5 modification sites per gene. The distribution of these m^{6}A modification sites on transcripts was mainly enriched in the coding sequence (CDS)

region, accounting for approximately 54%, followed by 3'UTR, accounting for ~44%, and only ~2% in 5'UTR **(Figure 2C)**. The distribution of normalized m^6A modification sites on transcripts showed that m^6A modification sites were enriched near the 3'UTR **(Figure 2D)**.

Analysis of the modification ratio of these modification sites revealed that overexpression of *PheALKBH9* reduced the overall m^6A modification level in rice **(Figure 2E)**, confirming the demethylation function of PheALKBH9. Through analysis of differential m^6A modification sites, we found that the majority of m^6A modification tended to be downregulated, with 5,387 hypo-methylated sites, while only 1,990 hyper-methylated sites **(Figure 2F,** Supplementary **Table S3)**. In addition, dot-blot results of total RNA verified that PheALKBH9 can reduce the m^6A level in rice **(Figure 2G)**. LC-MS/MS experiment of mRNA also confirmed the demethylation function of PheALKBH9 (Supplementary **Figure S3)**. The hypo-methylated m^6A peaks, primarily distributed in the CDS region (63%), were enriched near the stop codon **(**Supplementary **Figure S4)**. Gene Ontology (GO) analysis on genes only containing hypomethylated sites (henceforth 'hypo-methylated genes') revealed enrichment in gene expression, translation and oxidation-reduction reactions. In addition, hypo-methylated genes were also related to ribosome composition, oxidoreductase activity, translation factor activity and nucleic acid binding (**Figure 2H**). Furthermore, KEGG enrichment analysis revealed that hypo-methylated genes were mainly involved in the MAPK signaling pathway, plant-pathogen interactions, mRNA surveillance pathway, RNA transport and degradation (Supplementary **Figure S5**). Collectively, these results imply that PheALKBH9 may play a role in stress response through m^6A modification.

Identification of target RNAs bound by PheALKBH9 using the HyperTRIBE

To identify the RNAs bound by PheALKBH9, we fused a highly active catalytic domain, $ADARcd^{E488Q}$, to downstream of PheALKBH9 **(Figure 3A)**. The sequence of $ADARcd^{E488Q}$ was codon-optimized and cloned into the *UBI_{PRO}:PheALKBH9-$ADARcd^{E488Q}$-FLAG* vector (henceforth *OE-PheALKBH9-ADAR,* **Figure 3B**). Through Agrobacterium-mediated transformation of Kitaake callus, we obtained transgenic *OE-PheALKBH9-ADAR*. Simultaneously, we constructed an overexpression vector, *UBI_{PRO}:$ADARcd^{E488Q}$-FLAG*,

henceforth *OE-ADAR*, to express free ADAR^{E488Q} under the *UBI* promoter, serving as the control group to eliminate background noise. Western blot results of *OE-PheALKBH9-ADAR* (T0 generation) demonstrated the successful protein expression of line 10, 17, and 29 **(**Supplementary **Figure S6A)**. To confirm the function of *PheALKBH9*, we inoculated *OE-PheALKBH9-ADAR* with *Magnaporthe oryzae* Guy11 as well. *OE-PheALKBH9-ADAR*'s leaves exhibited more lesions than WT and *OE-ADAR* **(**Supplementary **Figure S6B)**, which was consistent with the phenotype of *OE-PheALKBH9* **(Figure 1H)**. DNA-based quantitative PCR with *M. oryzae Pot2* showed that the relative fungal biomass of *OE-PheALKBH9-ADAR* was also higher **(**Supplementary **Figure S6C)**. It demonstrated that overexpression of *PheALKBH9* reduces the resistance of rice to blast disease, no matter ADAR was expressed or not.

To identify PheALKBH9-target mRNAs, we extracted RNA from line10, 17, 29 of *OE-PheALKBH9-ADAR* in T0 generation and performed transcriptome sequencing (RNA-Seq) to detect A-G editing sites. The results showed that there was no obvious A-G editing site in WT and *OE-ADAR*. However, in lines 10, 17, and 29 of *OE-PheALKBH9-ADAR*, enrichment of A-G editing was observed. Subsequently, to exclude that these A-G editing sites were randomly edited by ADAR or naturally present in WT, we subtracted the A-G sites detected in WT and ADAR from the sites observed in *OE-PheALKBH9-ADAR*. After that, a large number of highly consistent editing sites were still observed in these three lines of *OE-PheALKBH9-ADAR* **(Figure 3C)**. We also found a high degree of overlap in the A-G editing sites between the three lines. The intersection contained 542 editing sites, and there were 2243 editing sites (corresponding to 2063 genes) identified in any two lines **(Figure 3D, left panel)**. The 2063 genes were used as PheALKBH9's target genes in the following analysis **(Figure 3D, right panel,** Supplementary **Table S4)**. As for the distribution of editing sites on genes, we found that they were mainly located in CDS and 3'UTR, and they were enriched around 3'UTR **(Figure 3, E and F)**, which was consistent with the enrichment trend of m^{6}A modification sites **(Figure 2D)**. GO enrichment analysis revealed that the 2063 genes were mainly related to oxidation-reduction, translation, and transport **(**Supplementary **Figure S7)**.

To validate the reliability of identified target RNAs bound by PheALKBH9, we collected T1 generation rice from line 10, 17, and 29 of *OE-PheALKBH9-ADAR*. Among them, line 17 and line 29, failed to enter the reproductive growth stage and died during the vegetative period, possibly due to abnormalities in growth and development caused by ADARcd^{E488Q}, which generated excessive editing sites. However, line 10, with relatively fewer editing sites, successfully produced T1 generation seeds. RNA-seq of T1 rice from line 10 revealed a significant enrichment of A-G editing sites and genes in *OE-PheALKBH9-ADAR* **(Figure 3, G and H)**. The A-G editing sites were also enriched in 3'UTR **(**Supplementary **Figure S8)**. Moreover, there was a high overlap with the editing genes between T1 and T0 generation rice, indicating the reliability of identified target RNAs **(Figure 3I)**.

There was a high overlap between PheALKBH9 target genes identified by HyperTRIBE and genes containing m^{6}A modification sites detected by Nanopore DRS. However, nearly half (1028 genes) of the 2063 PheALKBH9 target genes could not be detected by Nanopore DRS **(**Supplementary **Figure S9)**. We found that the expression level of the 1028 genes was relatively low. Due to the depth of Nanopore DRS, these low-expressed genes with binding sites cannot be detected for corresponding m^{6}A modification sites. Ultimately, we found that 286 PheALKBH9 binding genes exhibited a significant decrease at m^{6}A modification level **(Figure 3J)**.

Target RNAs Bound by PheALKBH9 in Bamboo

In order to identify the target RNAs bound by PheALKBH9 in Moso bamboo, we transiently expressed *35S$_{PRO}$:PheALKBH9-ADARcd^{E488Q}-FLAG* (henceforth '*OE-PheALKBH9-ADAR*') into bamboo protoplast via PEG-mediated transformation. Protoplasts expressing free ADARcd^{E488Q} (*35S$_{PRO}$:ADARcd^{E488Q}-FLAG,* henceforth '*OE-ADAR*') served as control **(Figure 3K)**. Protoplasts only transformed with vector pUC22 plasmid were named as empty vector (EV). After 24 hours of incubation, the protoplasts were collected respectively, followed by RNA-seq. After filtering out SNPs and excluding editing sites in the EV and *OE-ADAR* group, *OE-PheALKBH9-ADAR* showed significant enrichment of A-G editing sites **(Figure 3L,** Supplementary **Table S5)**.

We further performed orthologous analysis and found that the target genes identified in Moso

bamboo could be classified into 675 orthogroups, of which 117 orthogroups were consistent with the orthogroups identified in rice (corresponding to 134 genes) **(Figure 3M,** Supplementary **Table S6),** suggesting that some of the PheALKBH9's target genes were conserved in Moso bamboo and rice. Among the 134 target genes, the m^6A modification of 40 genes were hypo-regulated in *OE-PheALKBH9*. It has been reported that m^6A modification could regulate PAL in the transcript, which affects mRNA stability and translation. PABPC1 and PABPC4 can directly bind poly(A) tail to control PAL in human (Passmore and Coller, 2022). Our study found that PheALKBH9 can directly targeted *PABPC1* and *PABPC2* in both rice and bamboo based on HyperTRIBE data **(Figure 3M,** Supplementary **Table S6)**. Additionally, we detected a decrease in m^6A modification of *PABPC1* and *PABPC2* in *OE-PheALKBH9* **(Figure 3N)**, suggesting that PheALKBH9 may directly target *OsPABPC1* and *OsPABPC2* to regulate the PAL.

Changes in m^6A modifications affect gene expression levels only slightly

After identifying the target RNAs of PheALKBH9, we investigated the effect of PheALKBH9 on the transcription level. Transcriptome sequencing (RNA-seq) revealed that the overall gene expression level in *OE-PheALKBH9* was higher compared to WT **(**Supplementary **Figure S10A)**. Over 800 differentially expressed genes (DEGs) were identified between *OE-PheALKBH9* and WT, including 556 upregulated genes and 324 downregulated genes **(**Supplementary **Figure S10B,** Supplementary **Table S7)**. Both upregulated and downregulated genes were associated with oxidation-reduction, oxidoreductase activity, and peroxidase activity. Upregulated genes were also related to stress-associated fatty acid biosynthetic and metabolic processes. Additionally, some genes related to RNA modification, particularly pseudouridine modification, were identified among the upregulated genes. These findings suggest that *PheALKBH9* may alter the expression of numerous stress-related genes, including those involved in oxidation-reduction and fatty acid biosynthetic processes, thereby playing a role in plant resistance to stress **(**Supplementary **Figure S10C)**.

We performed correlation analysis of data from Nanopore DRS with RNA-seq and found that m^6A modification was negatively correlated with gene expression in both WT and *OE-*

PheALKBH9 **(**Supplementary **Figure S10, D and E)**. However, there was a little overlap between hyper-methylated and hypo-methylated genes with DEGs **(**Supplementary **Figure S10 F, G, and H)**, suggesting that m^6A modification regulated by PheALKBH9 only slightly alters the expression levels of the modified genes.

Genes with low m^6A modification tend to exhibit higher protein expression

In order to reveal the regulatory effect of *PheALKBH9* on protein expression, we performed data independent acquisition (DIA) mass spectrometry on WT and *OE-PheALKBH9* (lines 12 and 18), and it showed a positive correlation with the expression level from RNA-seq **(**Supplementary **Figure S11)**. We identified 604 differentially expressed proteins (DEPs) in *OE-PheALKBH9*, with 474 upregulated and 130 downregulated **(Figure 4, A and B,** Supplementary **Table S8)**. GO enrichment analysis showed that DEPs were mainly associated with oxidation-reduction reactions, oxidative stress, and response to external stimulus **(**Supplementary **Figure S12)**. KEGG analysis showed DEPs were mainly involved in flavonoid biosynthesis, MAPK signaling pathway, and plant-pathogen interactions, indicating that PheALKBH9 may play a key role in plant response to stress **(Figure 4C)**. We found genes that response to blast fungus, such as *Perox4* (Yang et al., 2021), *RSOsPR10* (Hashimoto et al., 2004), *OsCYP94D15*, and *OsBBI* (Li et al., 2011), were differentially expressed at both transcriptional and protein levels in *OE-PheALKBH9* **(Figure 4D)**. Subsequent RT-qPCR results confirmed the gene expression changes of these genes **(**Supplementary **Figure S13)**.

The m^6A modification was negatively correlated with protein level in both WT and *OE-PheALKBH9* **(Figure 4, E and F)**. There were 682 hyper-methylated genes in *OE-PheALKBH9*, among which only 21 genes and 5 genes showed upregulation and downregulation at the protein level, respectively **(Figure 4, G and H)**. However, the overlap ratio between hypo-methylated genes and DEPs increased. Among the 1794 hypo-methylated genes, 19 genes showed downregulated protein expression, while 61 genes showed upregulated protein expression **(Figure 4, I and J)**, which suggests that hypo-methylated genes favor higher protein expression.

Genes with low m^{6}A modification tend to exhibit shorter poly(A) tail length

The poly(A) tail length (PAL) is closely related to mRNA stability and translation. To reveal the effect of *PheALKBH9* on the PAL, we analyzed Nanopore DRS data and observed that transcripts in *OE-PheALKBH9* tended to have shorter PALs **(Figure 5A)**. In WT samples, the 25th and 75th percentile PALs were 70 and 115 nucleotides, respectively, while in *OE-PheALKBH9*, the corresponding values were 62 and 104 nucleotides **(Figure 5A)**. In *OE-PheALKBH9*, the PAL of 991 genes significantly shortened, while that of 39 genes significantly lengthened **(Figure 5B,** Supplementary **Table S9)**, indicating that overexpression of *PheALKBH9* tends to shorten PAL. GO analysis showed that genes with shortened PAL were mainly associated with translation, translational elongation, translation factor activity, and ribosomes **(Figure 5C)**, which was similar to the function of hypo-methylated genes. In addition, we found that the correlation between PAL and mRNA expression (based on RNA-seq data) was weak **(**Supplementary **Figure S14)**. And a negative correlation between protein expression and PAL was observed, but the correlation was low **(Figure 5D)**. However, a noticeable positive correlation between m^{6}A modification level and PAL was detected **(Figure 5E)**, indicating a potential regulation process between m^{6}A modification and PAL.

To gain deeper insights into the association between PAL and m^{6}A modification, we divided genes into three categories based on m^{6}A modification ratios: highly modified, moderately modified, and low-modified genes. Our analysis revealed that genes with high modification tended to show longer PAL, whereas those with low modification tended to have shorter PAL **(**Supplementary **Figure S15A and B)**. Specifically, the percentage of short PAL in the low-modification genes was increased in the *OE-PheALKBH9* **(**Supplementary **Figure S15, A and B)**. Additionally, the PAL of hypo-methylated genes was also shorter in *OE-PheALKBH9* **(**Supplementary **Figure S15C)**.

Previous studies reported that short PAL are associated with abundant and efficiently translated mRNA(Lima et al., 2017). Accordingly, we divided genes into three categories according to their protein expression level: high, medium, and low abundance. We observed

that genes with high protein expression tended to possess shorter PAL tails compared with low expressed genes **(**Supplementary **Figure S15, D and E)**. And PAL of the upregulated gene at protein expression level in *OE-PheALKBH9* was also shorter **(**Supplementary **Figure S15F)**.

For the genes with shortened PAL, their m^6A modifications were significantly lower than those with no significant changes in PAL **(Figure 5F)**. Among the 991 genes with shortened PAL, there was a large overlap (305 genes) with the 1794 hypo-methylated genes, suggesting that PAL reduction is significantly co-regulated with m^6A modification decline **(Figure 5G)**. *OsCAF1G* is a member of the CCR4-NOT complex that has deadenylation activity (Chou et al., 2017). Among the hypo-methylated genes and those with shortened PAL, we observed a reduction in both m^6A modification and PAL of *OsCAF1G* in *OE-PheALKBH9* (**Figure 5H**). Subsequently, m^6A-IP-qPCR was performed to validate that the m^6A modification of *OsCAF1G* mRNA was indeed reduced in *OE-PheALKBH9* (**Figure 5H**). This suggests that overexpression of *PheALKBH9* results in decreased m^6A methylation and PAL of *OsCAF1G*. In summary, it can be concluded that PAL has a positive correlation with the level of m^6A modification and has a negative correlation with the protein level expression of genes. Additionally, *PheALKBH9* appears to demethylate *OsCAF1G*, a component of CCR4-NOT complex, potentially influencing PAL modulation.

Impact of Transient Expression of *PheALKBH9* on the Bamboo Transcriptome

To explore the function of *PheALKBH9* in bamboo, we transiently transformed *PheALKBH9* using the bamboo mosaic virus (BaMV)-mediated expression system. Bamboo seedlings were transiently transformed with either PheALKBH9 or the control BaMV-P19-EGFP-2 vector. After one month, GFP observation **(**Supplementary **Figure S16A)** and western blot results confirmed successful expression of GFP-PheALKBH9 (~65 kDa) in the experimental group and GFP alone (~26 kDa) in the control **(**Supplementary **Figure S16B)**. RNA-seq analysis revealed significant upregulation of *PheALKBH9* in *OE-PheALKBH9* bamboo, indicating efficient virus-mediated transient transformation. We identified 1669 DEGs in *OE-PheALKBH9* bamboo **(**Supplementary **Figure S16C,** Supplementary **Table S10)**. Furthermore, we compared the DEGs induced by

PheALKBH9 in bamboo and rice, identifying 108 direct homologous groups **(**Supplementary **Figure S16D,** Supplementary **Table S11)**. GO enrichment analysis of the bamboo DEGs within these homologous groups revealed their involvement in stress response processes such as flavonoid and fatty acid biosynthesis **(**Supplementary **Figure S16E)**.

Among 1669 DEGs, which including 1085 upregulated genes and 584 downregulated genes **(**Supplementary **Figure S16C)**, GO enrichment of the upregulated genes revealed that they were mainly enriched in photosynthesis, seed germination, response to cytokinin, and response to oxidative stress **(**Supplementary **Figure S17A)**. The downregulated genes were associated with fungal resistance, peroxidase response, flavonoid biosynthesis, and stress response functions, and it was also involved in lignin biosynthesis and cell wall-related processes **(**Supplementary **Figure S17B)**.

PheALKBH9 binding to *Perox4* likely plays a role in blast disease

To further reveal the role of *PheALKBH9* in regulating blast resistance, we performed transcriptome sequencing of rice inoculated with Guy11 for 24 hours. In total, 1190 and 1165 genes were up-regulated and down-regulated, respectively. Most of these genes were enriched in oxidation reduction and response to biotic stimulus **(Supplementary Figure S18 A, B, Supplementary Table S12)**. Subsequently, we identified an overlap of 13 genes between the up-regulated genes, hypo-methylated genes, and target genes bound by PheALKBH9 **(Figure 6A, Supplementary Figure S18C)**. Among 13 genes, four are known to be involved in plant immune response: *Perox4* (Yang et al., 2021), *OsJAZ7*, *OsJAZ8* (Yamada et al., 2012), and *OsMETS2* (Zhai et al., 2022). RT-qPCR validation confirmed that these four genes were indeed upregulated in inoculated rice **(Figure 6B)**.

Perox4 negatively regulates the resistance to blast disease in rice by altering the expression of defense-related genes. The lesion size of the blast in *perox4* mutants was dramatically reduced compared with ZH11 (Yang et al., 2021). In this study, we observed a significant decrease in m^6A modification of *Perox4* in *OE-PheALKBH9*, as confirmed by m^6A-IP-qPCR, concurrent with upregulated gene expression and protein expression of *Perox4*. The browser view also

showed upregulated gene expression and decrease of m^6A modification of *Perox4* in *OE-PheALKBH9* (Figure 6C). In HyperTRIBE experiments, we detected A-G editing sites in the transcript of *OsPerox4*, confirming direct binding of PheALKBH9 to *OsPerox4* mRNA. Furthermore, leveraging AlphaFold3 (Abramson et al., 2024), we predicted the interaction between the PheALKBH9 protein and 100 nt RNA sequence surrounding the m^6A modification site of *Perox4*. Our analysis revealed a specific interaction where the main chain carbonyl oxygen atom (O) at position 154 of PheALKBH9 forms a hydrogen bond with the O2' of adenine within the RRACH motif of *Perox4* RNA **(Figure 6D)**.

Subsequently, we further explored whether PheALKBH9 regulates *Perox4* based on m^6A modification sites. Through nanopore sequencing, we identified one m^6A motif RRACH on *Perox4*, and cloned the sequence containing m^6A modification sites (255 bp) into the dual-luciferase reporter vector (named as the 'WT plasmid'). At the same time, the mutant plasmid where 'A' replaced with 'T' was constructed **(Figure 6E)**. WT or mutant plasmid was co-expressed with *$35S_{PRO}$:PheALKBH9-GFP* in tobacco via agrobacterium respectively. The results showed that firefly luciferase activity decreased in the mutant sample **(Figure 6, F and G)**. This suggested that PheALKBH9 potentially affected the protein level of Perox4 by binding to its m^6A motif.

In summary, our results demonstrate that overexpression of *PheALKBH9* decreases m^6A levels within *Perox4* transcripts, which positively regulated the transcription and protein expression of *Perox4*, crucial for the rice blast response. Additionally, PheALKBH9 exhibits binding affinity towards other genes involved in the response to blast fungal, such as *OsJAZ7* and *OsMETS2*, and similarly decreases their m^6A modification. This regulatory mechanism likely influences gene expression dynamics, thereby impacting rice's resistance against blast fungus **(Figure 6H)**. Our research provides essential insights into the role of m^6A modification and the regulatory functions of *PheALKBH9* in biotic stress.

Discussion

In recent years, the diverse functions of m^6A modification are emerging. In addition to playing a role in the growth and development of plants, m^6A modification also has important regulatory functions in plant response to stress, which is significant in adapting to complex and changing ecological environments. The writing, erasing, and reading of m^6A modifications are controlled by m^6A writer, eraser, and reader proteins respectively. In *Arabidopsis thaliana*, the expression levels of m^6A writer components, such as *MTA*, *MTB*, *FIP37*, and *VIR*, significantly increased after salt treatment, leading to an increase in global m^6A levels. The loss of *VIR* makes *Arabidopsis* more sensitive to salt stress (Hu et al., 2021). As components of m^6A erasers, ALKBH9B and ALKBH10B have m^6A demethylation activity in *Arabidopsis*. Depletion of *ALKBH10B* delayed flowering and inhibits vegetative growth in *Arabidopsis* (Duan et al., 2017), and it also makes *Arabidopsis* more sensitive to NaCl, mannitol, and ABA (Shoaib et al., 2021; Tang et al., 2021). *Arabidopsis* with impaired *ALKBH9B* does not show obvious developmental phenotypic changes but exhibits sensitivity to ABA (Tang et al., 2022). In this study, when *PheALKBH9B* is stably expressed in rice, it leads to increased susceptibility to rice blast disease, indicating that m^6A modification may be involved in regulating fungal infections in plants. We identified the modification site regulating the expression of *Perox4* within the CDS region. Therefore, we did not perform endogenous mutations on this A modification site, as it would result in amino acid changes. In the future, it would be worthwhile to investigate modification sites and binding sites located in the 3' UTR region. Using the CRISPR method to mutate these sites, we can assess their impact on gene function.

It has been reported that *AtALKBH9B* can positively regulate Alfalfa mosaic virus accumulation in *Arabidopsis* (Martinez-Perez et al., 2017). However, due to the difficulty in achieving stable transformation in bamboo, we were unable to obtain bamboo materials stably transformed with PheALKBH9. Therefore, further experiments are still needed to investigate the regulatory mechanism of PheALKBH9 in controlling BaMV infection in bamboo endogenously.

The HyperTRIBE method has facilitated the rapid identification of RBP targets, characterized by its simplicity, low cost, and wide applicability. Researchers successfully identified RNA

bound by ECT2 and ECT3 in *Arabidopsis* using the HyperTRIBE method (Arribas-Hernandez et al., 2021). Furthermore, HyperTRIBE has been utilized to identify target RNA of stress granule marker UBP1c in *Arabidopsis* and rice (Zhou et al., 2021). In this study, we identified 542 high-confidence A-G editing sites in *OE-PheALKBH9-ADAR* rice, thereby obtaining RNA targets bound by PheALKBH9. Recently, the high-efficiency RNA editing ability of ADARcd^{E488Q} in plants was verified by the interaction system of MCP-MS2 and AtGRP7 in rice and *Arabidopsis* protoplasts, respectively (Yin et al., 2023). Similarly, we achieved RNA editing in the target RNA of PheALKBH9 by overexpressing PheALKBH9-ADARcd in Moso bamboo protoplasts. This approach holds significant promise for tree species that are challenging to genetically transform, as it enables the straightforward acquisition of RBP target RNA through ADARcd editing in protoplasts.

ADAR-mediated mRNA editing may alter RNA stability or prematurely terminate translation, thereby affecting the function of mRNA, which could potentially impact plant growth and development, and stress responses. In this study, we successfully identified A-G editing sites in T0 transgenic rice overexpressing PheALKBH9-ADARcd. Interestingly, among the three lines with higher overexpression levels (10, 17, and 29), line 10 with a moderate number of editing sites continued to grow, while lines 17 and 29 with a large number of editing sites did not survive. This observation suggests that the abundance of A-G editing sites in plants may influence critical genes related to plant growth and development. As the number of editing sites increases, the instability of mRNA becomes more pronounced, thereby exerting a greater impact on plant physiology.

Currently, while DRS allows for the precise identification of m^6A modification sites at single nucleotide level, HyperTRIBE method edits adenines around the binding region, rather than at the binding site itself. In other words, the editing sites often do not coincide with the m^6A modification sites. To address this, we calculated the distance from the editing sites to the nearest m^6A modification site and found that this distance is primarily distributed within approximately 200 base pairs **(Supplementary Figure S19)**. This suggests that the true binding sites of

PheALKBH9 connected by HyperTRIBE mainly fall within this 200-base pair range. If combined with the precise single-nucleotide level m^6A modification sites, it would significantly aid in inferring the exact binding sites. However, whether this 200-base pair length is applicable to all RNA-binding proteins is currently unclear and requires specific analysis tailored to individual RNA-binding proteins.

It has been reported that m^6A modification regulates plant growth and resistance to stress by affecting protein translation. In strawberry, the m^6A writer components FvMTA may regulate fruit ripening by enhancing mRNA stability or translation efficiency of target genes involved in the ABA pathway (Zhou et al., 2021). In tomato, SlYTH2 represses the translation of target m^6A-modified mRNAs through the phase separation ability, which is critical for fruit aroma and quality (Bian et al., 2024). Overexpression of MhYTP2 enhanced the resistance to powdery mildew in apple, possibly by improving the translation efficiency of the antioxidant genes (Guo et al., 2022). In kiwifruit, m^6A demethylase AcALKBH10 modulates fruit ripening by altering mRNA stability and translation efficiency of critical genes (Su et al., 2024). In this study, we found that the m^6A modification was negatively correlated with protein expression in both WT and *OE-PheALKBH9* **(Figure 4, E and F)**. Hypo-methylated genes favor higher protein expression. For example, overexpression of *PheALKBH9* decreases m^6A levels of *Perox4* and positively regulated the transcription and protein expression of *Perox4*, which is crucial for the rice blast response. It suggests the potential regulatory role of m^6A on protein translation in plant immune responses.

Poly(A) tail length (PAL) is an important factor affecting mRNA stability and translation. Previous studies have reported potential links between m^6A and PAL. In *Trypanosoma brucei*, removal of a 16-mer cis-acting motif which is required for inclusion of m^6A in the poly(A) tail on VSG (variant surface glycoproteins) genes leads to the lacking of m^6A on poly(A) tails, rapid deadenylation and mRNA degradation (Viegas et al., 2022). In mouse embryonic stem cells, it has been found that m^6A-modified transcripts possess longer poly(A) tails (Liu et al., 2021). Similarly, in *Populus trichocarpa*, m^6A-modified transcripts tend to have longer PAL (Gao et al.,

2022). In this study, a noticeable positive correlation between m^6A modification level and PAL was detected **(Figure 5E)**, indicating a potential regulation between m^6A modification and PAL, which was consistent with the previous researche (Liu et al., 2021; Gao et al., 2022; Viegas et al., 2022). Based on the HyperTRIBE data, it can be seen that PheALKBH9 can directly targeted *PABPC1* and *PABPC2* (genes that regulate PAL in human) in both rice and bamboo **(Figure 3M, Supplementary Table S6)**. Additionally, we detected a decrease in m^6A modification of *PABPC1* and *PABPC2* in *OE-PheALKBH9* **(Figure 3N)**, suggesting that PheALKBH9 may target and demethylate *OsPABPC1* and *OsPABPC2* to regulate the PAL. Apart from that, *PheALKBH9* appears to demethylate *OsCAF1G*, a component of CCR4-NOT complex, potentially influencing PAL modulation. The evidence suggests that PheALKBH9 mediated-m^6A modification plays an important regulatory role on PAL.

Previous reports have shown that AtALKBH9B protein colocalizes with siRNA-body/P-body components, suggesting a functional association with posttranscriptional gene silencing (PTGS) or RNA degradation (Martinez-Perez et al., 2017). As an m^6A modification demethylase, AtALKBH9B is localized to stress granules (SGs) under heat in Arabidopsis (Fan et al., 2023). In this study, we found that PheALKBH9 contains disordered regions based on Predictor of Natural Disordered Regions (PONOR) (**Supplementary Figure S20A**), which is considered as a diagnosis of phase separation. In addition, we observed small granules in tobacco leaves that transiently overexpressing 35S:*PheALKBH9-GFP* (**Supplementary Figure S20B**). However, further experiment, like fluorescence recovery after photobleaching (FRAP) or other complementary assays, could be carried out in the future to confirm this phenomenon.

Our previous study revealed that RNA methylation inhibitor slightly reduced DNA methylation level, suggesting potential crosstalk between DNA and RNA methylation in plants (Liufu et al., 2023). Here, we reported the RNA m^6A demethylase function of PheALKBH9, though its impact on DNA methylation (e.g., 6mA or 5mC) remains unclear. As PheALKBH9 targets single-stranded RNA, direct DNA demethylation is low probability, but indirect regulation via DNA 6mA demethylase genes is plausible. Future studies could detect DNA 6mA

methylation in *OE-PheALKBH9* using specific method like nitrite sequencing (Mahdavi-Amiri et al., 2020), or DR-6mA-seq (Feng et al., 2024) to further explore the potential effect of PheALKBH9 on DNA methylation. In summary, the results provide perspective for analyzing the function of PheALKBH9 under stress.

Materials and methods

Identification of the Bamboo Demethylase Gene Family

To identify the m^6A demethylase gene family in Moso bamboo, we performed a BLASTP search for the 14 ALKBH family genes of Arabidopsis, with an E value less than 0.01 and at least 50% sequence identity. To ensure the accuracy of the identified ALKBH family genes of *Phyllostachys edulis*, we then downloaded the amino acid sequences of the conserved 2OG-FeII_Oxy_2 domain (PF13532) from the Pfam database (Mistry et al., 2021) and conducted a search using hmmsearch (Finn et al., 2011) with default parameters, retaining genes with an E-value less than 1E-5. Finally, we retained the ALKBH family genes of Moso bamboo identified by both BLASTP and hmmsearch. To infer the evolutionary relationship of ALKBH family genes, the protein sequences of human FTO and ALKBH5, the ALKBH family of rice and *Arabidopsis thaliana*, and the identified ALKBH family of *Phyllostachys edulis* were used to construct a phylogenetic tree using MEGAX (Kumar et al., 2018).

Genetic Transformation of *PheALKBH9* in Rice

All transgenic rice lines were generated in the background of Kitaake. We employed the Gateway cloning system to construct *$35S_{PRO}$:PheALKBH9-GFP* vector. The entry clone pDONR207 was used as an intermediate vector. Briefly, the CDS sequence of PheALKBH9 was cloned and inserted into the pGWB505 plasmid **(Supplementary Table S13, S14)**. The validated recombinant plasmid was transformed into *Agrobacterium tumefaciens* EHA105. We obtained rice seedlings through *Agrobacterium*-mediated transformation of rice calli. PCR amplification was carried out on genomic DNA using primers of the hygromycin gene to identify positive

transgenic rice **(Supplementary Table S13)**. RT-qPCR was performed with specific primers **(Supplementary Table S13)** to detect the mRNA expression level. The *OsActin* served as the reference gene. Western blot was used with an anti-GFP antibody to detect the protein expression of PheALKBH9 in transgenic rice.

Subcellular localization of PheALKBH9

The *35S$_{PRO}$:PheALKBH9-GFP* plasmid was transformed into *Agrobacterium tumefaciens* GV3101. After resuspending in MMA buffer (10 mM $MgCl_2$, 10 mM MES pH 5.6, 100 μM acetosyringone), the agrobacterium (OD=0.6) was injected into 4-week-old tobacco (*dcl2/4*). The plants were kept in the dark at 23°C for 24h and then were moved to normal light condition. After 48 hours of infection, GFP fluorescence was observed with a 488 nm laser line at 2% intensity using a Zeiss LSM 980 confocal microscope. Nuclei was stained using DAPI and was observed with a 405 nm laser line at 1.5% intensity. We obtained subcellular localization of PheALKBH9 to observe potential phase separation in the transformed tobacco.

m^{6}A dot blot

m^{6}A dot blot assay was used to detect total RNA modification changes in overexpressed materials. The procedure is briefly outlined as follows. Total RNA was extracted from the sample and adjusted to three concentration gradients: 2000 ng/μL, 1000 ng/μL, and 500 ng/μL. RNA was denatured at 95°C for 5 min and kept it on ice quickly. 2 μL RNA was spotted onto the nitrocellulose membranes (NC membranes) and air-dried naturally, then cross-linked under 302 nm UV light for 15 min. After crosslinking, the membrane was washed with TBST buffer for 5 min and subsequently blocked with 5% BSA for 1 h at room temperature. Then, washed the membrane with TBST buffer for 5 min and incubated with m^{6}A antibody for 1 h at room temperature. Subsequently, the membrane was washed 4 times with TBST buffer for 5 min each, followed by incubation with the corresponding secondary antibody IgG for 1 h at room temperature. The membrane was washed 4 times with TBST buffer for 5 min each and visualized using the ECL assay kit. After visualization, the membrane was stained in 0.02% methylene blue

solution for 30 minutes for nucleic acid quantification, followed by rinsing with water and photography.

Quantitative analysis of m^6A RNA modification by LC-MS

Total RNA was extracted from WT and *OE-PheALKBH9* leaves (3-week-old) using FastPure Universal Plant Total RNA Isolation Kit (Vazyme, Cat#RC411), respectively. Then mRNA was enriched using oligo dT Dynabeads (Invitrogen, Cat#61006). 200 ng mRNA was digested to single nucleosides with Nucleoside Digestion Mix (NEB, Cat#M0649S). Nucleosides were separated by ultra-performance liquid chromatography (UPLC) on an AB Sciex ExionLC™ system equipped with an Accucore™ C30 column (2.6 μm, 2.1 × 150 mm) and analyzed by triple quadrupole mass spectrometry (AB Sciex 4500 QQQ-MS). The m^6A/A ratio of sample was calculated based on peak areas of m^6A and A. The experiment was performed with two biological replicates. Data are given as the means ± SD (*t*-test, two-tailed).

Detecting Modification Changes in *OE-PheALKBH9*

Line 12 and 18 of *OE-PheALKBH9* were used as two replicates for nanopore direct RNA sequencing. For the DRS library, total RNA was extracted from seedlings and mRNA was extracted using oligo dT Dynabeads (Invitrogen, Cat#61006). 500 ng of poly(A) + RNA was used for the PCR-free library following the instructions of ONT RNA002 kit. The prepared libraries were sequenced on the MinION with R9.4 flow cells to generate fast5 files. Nanopore sequencing was performed using two MinION cells in total. After completing sequencing of the first DRS library for OE line 12, we performed flow cell washing using washing kit (ONT, EXP-WSH004) according to the instructions. This allowed us to remove the previous RNA sample and then refreshed the system for a new library from OE line 18. The two WT biological replicates were similarly processed and sequenced using the same protocol on a separate MinION flow cell.

After obtaining the raw data from Nanopore sequencing, the first step was to perform base

calling using guppy_basecaller (--flowcell FLO-MIN106 --kit SQK-RNA002) to identify the bases in the raw files. Next, the obtained FASTA file was corrected using lordec-correct (Salmela and Rivals, 2014) with corresponding Illumina data. Subsequently, tombo resquiggle (https://nanoporetech.github.io/tombo) was utilized to remap the identified bases to the transcripts. Finally, nanom^{6}A (Gao et al., 2021) was employed to identify m^{6}A modification sites. Sites with m^{6}A proportion greater than 1.2-fold (*OE-PheALKBH9*/Control) were considered as m^{6}A hyper-methylated sites, while those with a proportion less than 1/1.2 were considered as m^{6}A hypo-methylated sites. Genes only containing hyper-methylated sites were defined as hyper-methylated genes, while genes only containing hypo-methylated sites were defined as hypo-methylated genes. Hypomethylated & hypermethylated genes mean that contain both hypomethylated and hypermethylated sites due to multiple m^{6}A modification sites within the same gene.

Data-independent acquisition (DIA) proteomic analysis of *OE-PheALKBH9*

Line 12 and 18 of *OE-PheALKBH9* were used as independent replicates for data independent acquisition (DIA) mass spectrometry. Protein was lysed from leaf samples using lysis buffer (0.2% SDS, 0.1M Tris HCl, PH 7.6 ,10×Protease inhibitor), and quantified via BCA/Bradford assay. Proteins were incubated with 5 mM DTT (final concentration) at 56°C for 30 min, alkylated with 10 mM iodoacetamide (final concentration) in the dark for 30 min, and digested with trypsin (ratio 1:50) at 37°C for 16 h. Peptides were desalted using C18 StageTips and dried by vacuum centrifugation. The peptide segment (2 μg) was redissolved in solvent A (A: 0.1% formic acid solution) and then analyzed by LC-MS/MS using Orbitrap Fusion Lumos (Thermo Fisher).

DIA data was analyzed using Spectronaut (BGS Factory Settings) with default parameters. Peptide identifications were filtered at 1% FDR. By filtering out common contaminating proteins and their peptides, we obtained the identified peptides and protein. Differential proteins were defined using thresholds of FC > 1.2 with $p < 0.05$.

Detecting Poly(A) Tail Length Changes in *OE-PheALKBH9*

Using nanopolish (v0.13.2) (Workman et al., 2019), the original electrical signal of each read was utilized to predict the length of poly(A) tails. Only reads with the QC tag "PASS" were selected for downstream analysis. Subsequently, featureCounts (v2.0.1) was employed in long-read mode to assign each read to its corresponding gene (Liao et al., 2014), retaining only reads that can be assigned to a specific gene for downstream analysis. The Poly(A) tail length (PAL) of each gene was defined as the median of all reads supporting the gene, with at least three valid reads supporting the gene required for downstream analysis. Wilcoxon rank-sum test was performed to obtain p-values for PAL differences between different samples, with a threshold of PAL fold change greater than 1.25 and p-value less than 0.05 considered significant.

m^6A-IP-qPCR

The procedure followed in this study was based on the previously described method (Dominissini et al., 2013). Briefly, 50 μg of total RNA was fragmented into 100–200 nt using RNA Fragmentation Reagents (Invitrogen, Cat#AM8740), followed by collecting with Zymo-Spin™ IC Column (Zymo, Cat#R1015). Subsequently, 10% of the eluted RNA served as the input sample, while the remaining RNA was incubated with 5 μg of m^6A antibody (NEB, Cat#E1611AVIAL) in 100 μL of IP buffer (150 mM NaCl, 0.1% Igepal CA-630, 10 mM Tris–HCl, pH 7.4, 40 U RiboLock RNase Inhibitor) at 4 °C for 4 h. The fragmented RNA-antibody complexes were subsequently incubated with protein A+G magnetic beads (sigma, #16-663) for 2h, and RNA was collected with Zymo-Spin™ IC Column (Zymo, #R1015). Both input and IP samples were analyzed by RT-qPCR using specific primers (**Supplementary Table S13**). The relative enrichment of m^6A was calculated by normalizing the the Cycle Threshold (CT) value of the IP sample to that of input sample. A modified RNA (**Supplementary Table S14**), was synthesized and used as an internal reference.

Identifying Endogenous Target RNAs Bound by PheALKBH9

To identify endogenous target RNA bound to PheALKBH9, the following steps were conducted.

The codon of ADARcd^{E488Q} is optimized for better expression in rice and then fused to the C-terminus of PheALKBH9 **(Supplementary Table S14)**. The fused fragment was ligated into the KpnI-digested pCUbi1390 vector to generate the final construct *UBI_{PRO}: PheALKBH9-ADARcd^{E488Q}-FLAG*. We transformed the recombinant plasmid into Kitaake calli by *Agrobacterium*-mediated T-DNA insertion. PCR amplification was carried out on genomic DNA using primers of the hygromycin gene to identify positive transgenic rice **(Supplementary Table S13)**. RT-qPCR was performed with specific primers **(Supplementary Table S13)** to detect the mRNA expression level. The *OsActin* served as the reference gene. Western blot was used with an anti-FLAG antibody to detect the protein expression in transgenic rice. We collected the leaf tissues from the T0 transgenic rice plants with high expression level and extracted RNA with a Total RNA Extraction Kit (Tiangen, DP#441). RNA-seq was carried out for identification of target RNA bound to PheALKBH9 by detecting A-G mutation sites.

Endogenous target binding sites of PheALKBH9 in Moso bamboo were identified using PEG-mediated transient transformation with protoplasts. To identify the target RNA, ADARcd^{E488Q} was fused with PheALKBH9 under the control of 35S promoter (*$35S_{PRO}$: PheALKBH9-ADARcd^{E488Q}-FLAG*) in the pUC22 vector and expressed in bamboo protoplasts. In the pUC22 vector, GFP was driven by another 35S promotor which was used to test the transformation efficiency of protoplasts. Bamboo protoplast isolation and transformation were performed as described previously (Wang et al., 2019).

The analysis pipeline for HyperTRIBE in rice and Moso bamboo mainly followed the previous method (Zhou et al., 2021). In brief, the transcriptome was aligned to the genome using HISAT2, then SNP sites were identified using the GATK4 pipeline, and sites with less than 10 supporting reads and a mutation ratio greater than 90% were filtered out. Finally, A-G mutation sites were considered as candidate editing sites for the gene. The rice genome and annotation were OsativaKitaake_499_v3.1 (Jain et al., 2019), and the Moso bamboo genome 2.0 (Zhao et al., 2018).

Testing Transgenic Seedlings for Resistance to Rice Blast Disease

To test the resistance of transgenic rice seedlings to rice blast disease, the following steps were undertaken. *M.oryzae* strain Guy11 was cultured on a complete medium (CM) as previously described (Kong et al., 2024). Seedlings of transgenic rice were cultured for 3 weeks in a greenhouse at 28 °C according to the hydroponic method. We adjusted the spore concentration of *M. oryzae* to 4×10^5 spores/ml using a hemocytometer. The suspension of *M. oryzae* was evenly sprayed on the leaves of rice in a moist (85% humidity) and dark chamber. After incubating in the dark chamber with 85% humidity for 24 hr, the inoculated seedlings were cultured in growth chambers at 26 °C under a 16-hr light/8-hr dark cycle with 85% humidity. After 3-4 days, the rice blast lesions were evaluated and photographed. For quantitative analysis, leaf samples of the inoculated rice were collected for DNA extraction. The fungal biomass was examined by qPCR using *Pot2* primers of *M. oryzae*. *OsActin* was used as the reference gene.

Transient Transformation of Bamboo Seedlings Using a Virus-Based System

To explore the function of PheALKBH9 in bamboo, we transiently transformed PheALKBH9 with the bamboo mosaic virus (BaMV)-mediated expression system (Jin et al., 2023). We cloned the coding sequence of *PheALKBH9* and inserted it into BaMV-P19-EGFP-2 vector. The recombinant vector *35S$_{PRO}$:GFP-PheALKBH9* was transferred to the leaves of *NbDCL2/4* by Agrobacterium strain GV3101. Seven days later, we ground the infiltrated leaves into infectious juice with 1× phosphate-buffered saline (PBS) and emery to inoculate 2-week-old Moso bamboo leaves mechanically. After 2 d of moisturizing culture, the bamboo seedlings with BaMV-infected were transferred to normal growth conditions at 25°C. *BaMV-P19-EGFP-2* overexpression lines of bamboo served as the control.

Differential gene expression analysis in PheALKBH9-overexpressing rice and bamboo

Total RNA was extracted from WT and OE-PheALKBH9 in rice, as well as from OE-GFP (empty vector control, EV group) and OE-PheALKBH9 in bamboo. Then mRNA was isolated for dUTP strand-specific transcriptome sequencing. For the analysis of DEGs, the following RNA-seq data processing pipeline was implemented. We constructed strand-specific RNA-seq

libraries using the dUTP method and aligned the raw transcriptome data to the reference genome using HISAT2 (Kim et al., 2019) (with parameters --rna-strandness RF and default parameters). Subsequently, duplicate reads were removed using sambamba markdup (Tarasov et al., 2015). Gene expression was quantified using StringTie (Pertea et al., 2015) and differential expression analysis was performed with DESeq2 (Love et al., 2014). Finally, DEGs were identified based on the following criteria: adjusted p-value (p-adj) less than 0.05 and fold change (FC) greater than 1.5.

GO and KEGG Enrichment Analysis

For the GO enrichment analysis of rice, agriGO v2.0 database was utilized. This analysis identified enriched GO terms associated with the DEGs. Significantly enriched terms were those with a False Discovery Rate (FDR) less than 0.05. As for bamboo, the GO annotation file was obtained using BLAST2GO. Subsequently, clusterProfiler was employed to perform GO enrichment analysis for bamboo (Wu et al., 2021). Similarly, significantly enriched GO terms were identified based on an FDR threshold of less than 0.05. In addition, KEGG enrichment analysis was achieved using KOBAS (Xie et al., 2011).

Dual luciferase assay

The 255 bp sequence around m^6A modification site on CDS of *Perox4* was cloned into pGreenII 0800-LUC vector of dual luciferase reporter system (labeled as WT vector), and a mutant 255 bp sequence which replaced the 'A' base of RRACH with 'T' was cloned into pGreenII 0800-LUC (labeled as mutant vector). The WT and mutant vectors were separately introduced into Agrobacterium *GV3101*. Each strain was then mixed in a 1:1 (v/v) ratio with Agrobacterium expressing *$35S_{PRO}$:PheALKBH9-GFP* for tobacco infiltration. Tobacco leaves were harvested 48 hours after agroinfiltration. Luciferase activity was measured using the Tanon 5200 Imaging System (Tanon, China). Leaf samples were ground in liquid nitrogen and lysed in 1× Passive Lysis Buffer (Promega). The lysates were centrifuged at 12,000 × g for 10 min at 4°C, and the supernatants were collected for analysis. Luciferase activity was quantified using the Luciferase

Assay System (Promega, Cat. No. E1500) according to the manufacturer's protocol. The experiment was repeated three times independently, with six tobacco plants (*dcl2/4*) analyzed per replicate.

Statistical analysis

Quantification analysis and significance test were applied for RT-qPCR, meRIP-qPCR and plant physiological measurements using Python (3.8), R (4.2) and Prism. Data are given as the means ± SD unless stated otherwise. Statistical significance was assessed using Student's t-test (two-tailed) and Mann–Whitney U tests. For each figure, the legend specifies the test used and the exact n.

Data Availability

The raw sequence data reported in this paper have been deposited in the Genome Sequence Archive in the National Genomics Data Center (Nucleic Acids Res 2022), China National Center for Bioinformation/Beijing Institute of Genomics, Chinese Academy of Sciences (GSA: CRA015555, OMIX: OMIX006084) that are publicly accessible at https://ngdc.cncb.ac.cn/gsa and https://ngdc.cncb.ac.cn/omix.

Accession Numbers

The bamboo sequence of *PheALKBH9* (PH02Gene00238) can be found in Supplementary Table S14. The kitaake sequence data for the genes analyzed in this study are available in the KitaakeX Mutant Database (https://kitbase.ucdavis.edu/home) under the respective accession numbers: *OsPABPC1*, OsKitaake09g007000, LOC_Os09g02700; *OsPABPC2,* OsKitaake08g110700, LOC_Os08g22354; *Perox4*, OsKitaake07g273000, LOC_Os07g48020; *RSOsPR10,* OsKitaake12g173600, LOC_Os12g36830; *OsCAF1G,* OsKitaake09g099900, LOC_Os09g24990; *OsJAZ7*, OsKitaake07g229000, LOC_Os07g42370; *OsMETS2,*

OsKitaake12g217600, LOC_Os12g42884; *OsJAZ8*, OsKitaake09g114100, LOC_Os09g26780; *OsCYP94D15*, OsKitaake03g094400, LOC_Os03g12260; *OsBBI*, OsKitaake03g395700, LOC_Os03g60840; *OsCYP71Z2*, OsKitaake07g074400, LOC_Os07g11739; *OsPIP1;3*, OsKitaake02g389000, LOC_Os02g57720; *OsGLP8-4*, OsKitaake08g057200, LOC_Os08g08980; *Oxidoreductase*, OsKitaake04g146400, LOC_Os04g37490; *Peroxidase*, OsKitaake06g128400, LOC_Os06g20150; *OsCYP71Z2*, OsKitaake07g074400, LOC_Os07g11739.

Acknowledgments

We would like to acknowledge the technical support from Instrumental Analysis Center of Fujian Agriculture and Forestry University.

Funding

This research was funded by the National Key R&D Program of China (2021YFD2200505), the National Natural Science Foundation of China (32371980), the Natural Science Foundation of Fujian Province (2025J02014), the S&T Innovation (KFB23180 and KFB24096A) and the Forestry Peak Discipline Construction Project of Fujian Agriculture and Forestry University (725025010 and 72202200205).

AUTHOR CONTRIBUTIONS

L.G. conceived this project and designed the experiments. HHW., TL., YJ., SY., YJ., ZZ., WB., HZ., LZ., HZ., carried out the experiments. HYW performed bioinformatics analysis. HHW., HYW., and L.G. wrote the manuscript. CL., and ASNR edited the manuscript. All authors contributed to the article and approved the submitted version.

DECLARATION OF INTERESTS

The authors declare that they have no competing interests.

REFERENCES

Abramson J, Adler J, Dunger J, Evans R, Green T, Pritzel A, Ronneberger O, Willmore L, Ballard AJ, Bambrick J, Bodenstein SW, Evans DA, Hung CC, O'Neill M, Reiman D, Tunyasuvunakool K, Wu Z, Zemgulyte A, Arvaniti E, Beattie C, Bertolli O, Bridgland A, Cherepanov A, Congreve M, Cowen-Rivers AI, Cowie A, Figurnov M, Fuchs FB, Gladman H, Jain R, Khan YA, Low CMR, Perlin K, Potapenko A, Savy P, Singh S, Stecula A, Thillaisundaram A, Tong C, Yakneen S, Zhong ED, Zielinski M, Zidek A, Bapst V, Kohli P, Jaderberg M, Hassabis D, Jumper JM (2024) Accurate structure prediction of biomolecular interactions with AlphaFold 3. Nature **630:** 493-500

Arribas-Hernandez L, Rennie S, Schon M, Porcelli C, Enugutti B, Andersson R, Nodine MD, Brodersen P (2021) The YTHDF proteins ECT2 and ECT3 bind largely overlapping target sets and influence target mRNA abundance, not alternative polyadenylation. Elife **10**

Bian H, Song P, Gao Y, Deng Z, Huang C, Yu L, Wang H, Ye B, Cai Z, Pan Y, Wang F, Liu J, Gao X, Chen K, Jia G, Klee HJ, Zhang B (2024) The m^6A reader SlYTH2 negatively regulates tomato fruit aroma by impeding the translation process. Proc Natl Acad Sci U S A **121:** e2405100121

Boccaletto P, Stefaniak F, Ray A, Cappannini A, Mukherjee S, Purta E, Kurkowska M, Shirvanizadeh N, Destefanis E, Groza P, Avsar G, Romitelli A, Pir P, Dassi E, Conticello SG, Aguilo F, Bujnicki JM (2022) MODOMICS: a database of RNA modification pathways. 2021 update. Nucleic Acids Res **50:** D231-D235

Chou WL, Chung YL, Fang JC, Lu CA (2017) Novel interaction between CCR4 and CAF1 in rice CCR4-NOT deadenylase complex. Plant Mol Biol **93:** 79-96

Dominissini D, Moshitch-Moshkovitz S, Salmon-Divon M, Amariglio N, Rechavi G (2013) Transcriptome-wide mapping of N^6-methyladenosine by m^6A-seq based on immunocapturing and massively parallel sequencing. Nat Protoc **8:** 176-189

Duan HC, Wei LH, Zhang C, Wang Y, Chen L, Lu Z, Chen PR, He C, Jia G (2017) ALKBH10B Is an RNA N^6-Methyladenosine Demethylase Affecting Arabidopsis Floral Transition. Plant Cell **29:** 2995-3011

Fan W, Wang L, Lei Z, Li H, Chu J, Yan M, Wang Y, Wang H, Yang J, Cho J (2023) m^6A RNA demethylase AtALKBH9B promotes mobilization of a heat-activated long terminal repeat retrotransposon in Arabidopsis. Sci Adv **9:** eadf3292

Feng X, Cui X, Zhang LS, Ye C, Wang P, Zhong Y, Wu T, Zheng Z, He C (2024) Sequencing of N^6-methyl-deoxyadenosine at single-base resolution across the mammalian genome. Mol Cell **84:** 596-610 e596

Finn RD, Clements J, Eddy SR (2011) HMMER web server: interactive sequence similarity searching. Nucleic Acids Res **39:** W29-37

Furci L, Berthelier J, Saze H (2024) RNA N^6-adenine methylation dynamics impact Hyaloperonospora arabidopsidis resistance in Arabidopsis. Plant Physiol **196:** 745-753

Gao Y, Liu X, Jin Y, Wu J, Li S, Li Y, Chen B, Zhang Y, Wei L, Li W (2022) Drought induces epitranscriptome and proteome changes in stem-differentiating xylem of *Populus trichocarpa*. Plant Physiology **190:** 459-479

Gao Y, Liu X, Wu B, Wang H, Xi F, Kohnen MV, Reddy ASN, Gu L (2021) Quantitative profiling of N^6-methyladenosine at single-base resolution in stem-differentiating xylem of *Populus trichocarpa* using Nanopore direct RNA sequencing. Genome Biol **22:** 22

Guo T, Liu C, Meng F, Hu L, Fu X, Yang Z, Wang N, Jiang Q, Zhang X, Ma F (2022) The m^6A reader MhYTP2 regulates *MdMLO19* mRNA stability and antioxidant genes translation efficiency conferring powdery mildew resistance in apple. Plant Biotechnol J **20:** 511-525

Hashimoto M, Kisseleva L, Sawa S, Furukawa T, Komatsu S, Koshiba T (2004) A novel rice PR10 protein, RSOsPR10, specifically induced in roots by biotic and abiotic stresses, possibly via the jasmonic acid signaling pathway. Plant Cell Physiol **45:** 550-559

Hu J, Cai J, Park SJ, Lee K, Li Y, Chen Y, Yun JY, Xu T, Kang H (2021) N^6-Methyladenosine mRNA methylation is important for salt stress tolerance in Arabidopsis. Plant J **106:** 1759-1775

Jain R, Jenkins J, Shu S, Chern M, Martin JA, Copetti D, Duong PQ, Pham NT, Kudrna DA, Talag J, Schackwitz WS, Lipzen AM, Dilworth D, Bauer D, Grimwood J, Nelson CR, Xing F, Xie W, Barry KW, Wing RA, Schmutz J, Li G, Ronald PC (2019) Genome sequence of the model rice variety KitaakeX. BMC Genomics **20:** 905

Jia G, Fu Y, Zhao X, Dai Q, Zheng G, Yang Y, Yi C, Lindahl T, Pan T, Yang YG, He C (2011) N^6-methyladenosine in nuclear RNA is a major substrate of the obesity-associated FTO. Nat Chem Biol **7:** 885-887

Jin Y, Wang B, Bao M, Li Y, Xiao S, Wang Y, Zhang J, Zhao L, Zhang H, Hsu YH, Li M, Gu L (2023) Development of an efficient expression system with large cargo capacity for interrogation of gene function in bamboo based on bamboo mosaic virus. J Integr Plant Biol **65:** 1369-1382

Kim D, Paggi JM, Park C, Bennett C, Salzberg SL (2019) Graph-based genome alignment and genotyping with HISAT2 and HISAT-genotype. Nat Biotechnol **37:** 907-915

Kong Y, Guo P, Xu J, Li J, Wu M, Zhang Z, Wang Y, Liu X, Yang L, Liu M, Zhang H, Wang P, Zhang Z (2024) MoMkk1 and MoAtg1 dichotomously regulating autophagy and pathogenicity through MoAtg9 phosphorylation in *Magnaporthe oryzae*. mBio **15:** e0334423

Kumar S, Stecher G, Li M, Knyaz C, Tamura K (2018) MEGA X: Molecular Evolutionary Genetics Analysis across Computing Platforms. Mol Biol Evol **35:** 1547-1549

Li W, Zhong S, Li G, Li Q, Mao B, Deng Y, Zhang H, Zeng L, Song F, He Z (2011) Rice RING protein OsBBI1 with E3 ligase activity confers broad-spectrum resistance against *Magnaporthe oryzae* by modifying the cell wall defence. Cell Res **21:** 835-848

Liao Y, Smyth GK, Shi W (2014) featureCounts: an efficient general purpose program for assigning sequence reads to genomic features. Bioinformatics **30:** 923-930

Lima SA, Chipman LB, Nicholson AL, Chen YH, Yee BA, Yeo GW, Coller J, Pasquinelli AE (2017) Short poly(A) tails are a conserved feature of highly expressed genes. Nat Struct Mol Biol **24:** 1057-1063

Liu Y, Zhang Y, Lu F, Wang J (2021) Interactions between RNA m^6A modification, alternative splicing, and poly (A) tail revealed by MePAIso-seq2. bioRxiv**:** 2021.2008. 2029.458071

Liufu Y, Xi F, Wu L, Zhang Z, Wang H, Wang H, Zhang J, Wang B, Kou W, Gao J, Zhao L, Zhang H, Gu L

(2023) Inhibition of DNA and RNA methylation disturbs root development of moso bamboo. Tree Physiol **43:** 1653-1674

Love MI, Huber W, Anders S (2014) Moderated estimation of fold change and dispersion for RNA-seq data with DESeq2. Genome Biol **15:** 550

Mahdavi-Amiri Y, Chung Kim Chung K, Hili R (2020) Single-nucleotide resolution of N^6-adenine methylation sites in DNA and RNA by nitrite sequencing. Chem Sci **12:** 606-612

Martinez-Perez M, Aparicio F, Lopez-Gresa MP, Belles JM, Sanchez-Navarro JA, Pallas V (2017) Arabidopsis m^6A demethylase activity modulates viral infection of a plant virus and the m^6A abundance in its genomic RNAs. Proc Natl Acad Sci U S A **114:** 10755-10760

Mistry J, Chuguransky S, Williams L, Qureshi M, Salazar GA, Sonnhammer ELL, Tosatto SCE, Paladin L, Raj S, Richardson LJ, Finn RD, Bateman A (2021) Pfam: The protein families database in 2021. Nucleic Acids Res **49:** D412-D419

Passmore LA, Coller J (2022) Roles of mRNA poly(A) tails in regulation of eukaryotic gene expression. Nat Rev Mol Cell Biol **23:** 93-106

Pertea M, Pertea GM, Antonescu CM, Chang TC, Mendell JT, Salzberg SL (2015) StringTie enables improved reconstruction of a transcriptome from RNA-seq reads. Nat Biotechnol **33:** 290-295

Prall W, Sheikh AH, Bazin J, Bigeard J, Almeida-Trapp M, Crespi M, Hirt H, Gregory BD (2023) Pathogen-induced m^6A dynamics affect plant immunity. Plant Cell **35:** 4155-4172

Ramanathan M, Porter DF, Khavari PA (2019) Methods to study RNA-protein interactions. Nat Methods **16:** 225-234

Ruzicka K, Zhang M, Campilho A, Bodi Z, Kashif M, Saleh M, Eeckhout D, El-Showk S, Li H, Zhong S, De Jaeger G, Mongan NP, Hejatko J, Helariutta Y, Fray RG (2017) Identification of factors required for m^6A mRNA methylation in Arabidopsis reveals a role for the conserved E3 ubiquitin ligase HAKAI. New Phytol **215:** 157-172

Salmela L, Rivals E (2014) LoRDEC: accurate and efficient long read error correction. Bioinformatics **30:** 3506-3514

Shen L, Liang Z, Gu X, Chen Y, Teo ZW, Hou X, Cai WM, Dedon PC, Liu L, Yu H (2016) N^6-Methyladenosine RNA Modification Regulates Shoot Stem Cell Fate in Arabidopsis. Dev Cell **38:** 186-200

Shi H, Wei J, He C (2019) Where, When, and How: Context-Dependent Functions of RNA Methylation Writers, Readers, and Erasers. Mol Cell **74:** 640-650

Shoaib Y, Hu J, Manduzio S, Kang H (2021) Alpha-ketoglutarate-dependent dioxygenase homolog 10B, an N^6-methyladenosine mRNA demethylase, plays a role in salt stress and abscisic acid responses in *Arabidopsis thaliana*. Physiol Plant **173:** 1078-1089

Su D, Shu P, Hu N, Chen Y, Wu Y, Deng H, Du X, Zhang X, Wang R, Li H, Zeng Y, Li D, Xie Y, Li M, Hong Y, Liu K, Liu M (2024) Dynamic m^6A mRNA methylation reveals the involvement of AcALKBH10 in ripening-related quality regulation in kiwifruit. New Phytol **243:** 2265-2278

Tang J, Lei D, Yang J, Chen S, Wang X, Huang X, Zhang S, Cai Z, Zhu S, Wan J, Jia G (2024) OsALKBH9-mediated m^6A demethylation regulates tapetal PCD and pollen exine accumulation in rice. Plant Biotechnol J

Tang J, Yang J, Duan H, Jia G (2021) ALKBH10B, an mRNA m^6A Demethylase, Modulates ABA Response During Seed Germination in Arabidopsis. Front Plant Sci **12:** 712713

Tang J, Yang J, Lu Q, Tang Q, Chen S, Jia G (2022) The RNA N^6-methyladenosine demethylase ALKBH9B modulates ABA responses in Arabidopsis. J Integr Plant Biol **64:** 2361-2373

Tarasov A, Vilella AJ, Cuppen E, Nijman IJ, Prins P (2015) Sambamba: fast processing of NGS alignment formats. Bioinformatics **31:** 2032-2034

Vasupalli N, Hou D, Singh RM, Wei H, Zou LH, Yrjala K, Wu A, Lin X (2021) Homo- and Hetero-Dimers of CAD Enzymes Regulate Lignification and Abiotic Stress Response in Moso Bamboo. Int J Mol Sci **22**

Vespa L, Vachon G, Berger F, Perazza D, Faure JD, Herzog M (2004) The immunophilin-interacting protein AtFIP37 from Arabidopsis is essential for plant development and is involved in trichome endoreduplication. Plant Physiol **134:** 1283-1292

Viegas IJ, de Macedo JP, Serra L, De Niz M, Temporão A, Silva Pereira S, Mirza AH, Bergstrom E, Rodrigues JA, Aresta-Branco F (2022) N^6-methyladenosine in poly (A) tails stabilize VSG transcripts. Nature **604:** 362-370

Wang C, Yang J, Song P, Zhang W, Lu Q, Yu Q, Jia G (2022) FIONA1 is an RNA N^6-methyladenosine methyltransferase affecting Arabidopsis photomorphogenesis and flowering. Genome Biology **23:** 40

Wang Y, Gao Y, Zhang H, Wang H, Liu X, Xu X, Zhang Z, Kohnen MV, Hu K, Wang H, Xi F, Zhao L, Lin C, Gu L (2019) Genome-Wide Profiling of Circular RNAs in the Rapidly Growing Shoots of Moso Bamboo (*Phyllostachys edulis*). Plant Cell Physiol **60:** 1354-1373

Workman RE, Tang AD, Tang PS, Jain M, Tyson JR, Razaghi R, Zuzarte PC, Gilpatrick T, Payne A, Quick J, Sadowski N, Holmes N, de Jesus JG, Jones KL, Soulette CM, Snutch TP, Loman N, Paten B, Loose M, Simpson JT, Olsen HE, Brooks AN, Akeson M, Timp W (2019) Nanopore native RNA sequencing of a human poly(A) transcriptome. Nat Methods **16:** 1297-1305

Wu T, Hu E, Xu S, Chen M, Guo P, Dai Z, Feng T, Zhou L, Tang W, Zhan L, Fu X, Liu S, Bo X, Yu G (2021) clusterProfiler 4.0: A universal enrichment tool for interpreting omics data. Innovation (Camb) **2:** 100141

Xie C, Mao X, Huang J, Ding Y, Wu J, Dong S, Kong L, Gao G, Li CY, Wei L (2011) KOBAS 2.0: a web server for annotation and identification of enriched pathways and diseases. Nucleic Acids Res **39:** W316-322

Xu T, Wu X, Wong CE, Fan S, Zhang Y, Zhang S, Liang Z, Yu H, Shen L (2022) FIONA1-mediated m^6A modification regulates the floral transition in Arabidopsis. Advanced Science **9:** 2103628

Xu W, Rahman R, Rosbash M (2018) Mechanistic implications of enhanced editing by a HyperTRIBE RNA-binding protein. RNA **24:** 173-182

Yamada S, Kano A, Tamaoki D, Miyamoto A, Shishido H, Miyoshi S, Taniguchi S, Akimitsu K, Gomi K (2012) Involvement of OsJAZ8 in jasmonate-induced resistance to bacterial blight in rice. Plant Cell Physiol **53:** 2060-2072

Yang D, Li S, Xiao Y, Lu L, Zheng Z, Tang D, Cui H (2021) Transcriptome analysis of rice response to blast fungus identified core genes involved in immunity. Plant Cell Environ **44:** 3103-3121

Yin S, Chen Y, Chen Y, Xiong L, Xie K (2023) Genome-wide profiling of rice Double-stranded RNA-Binding Protein 1-associated RNAs by targeted RNA editing. Plant Physiol **192:** 805-820

Yu Q, Liu S, Yu L, Xiao Y, Zhang S, Wang X, Xu Y, Yu H, Li Y, Yang J, Tang J, Duan HC, Wei LH, Zhang H, Wei J, Tang Q, Wang C, Zhang W, Wang Y, Song P, Lu Q, Zhang W, Dong S, Song B, He C, Jia G (2021) RNA demethylation increases the yield and biomass of rice and potato plants in field trials. Nat Biotechnol **39:** 1581-1588

Yue Y, Liu J, He C (2015) RNA N^6-methyladenosine methylation in post-transcriptional gene expression

regulation. Genes Dev **29:** 1343-1355

Zhai K, Liang D, Li H, Jiao F, Yan B, Liu J, Lei Z, Huang L, Gong X, Wang X, Miao J, Wang Y, Liu JY, Zhang L, Wang E, Deng Y, Wen CK, Guo H, Han B, He Z (2022) NLRs guard metabolism to coordinate pattern- and effector-triggered immunity. Nature **601:** 245-251

Zhang F, Zhang YC, Liao JY, Yu Y, Zhou YF, Feng YZ, Yang YW, Lei MQ, Bai M, Wu H, Chen YQ (2019) The subunit of RNA N^6-methyladenosine methyltransferase OsFIP regulates early degeneration of microspores in rice. PLoS Genet **15:** e1008120

Zhao H, Gao Z, Wang L, Wang J, Wang S, Fei B, Chen C, Shi C, Liu X, Zhang H, Lou Y, Chen L, Sun H, Zhou X, Wang S, Zhang C, Xu H, Li L, Yang Y, Wei Y, Yang W, Gao Q, Yang H, Zhao S, Jiang Z (2018) Chromosome-level reference genome and alternative splicing atlas of moso bamboo (*Phyllostachys edulis*). Gigascience **7**

Zheng G, Dahl JA, Niu Y, Fedorcsak P, Huang CM, Li CJ, Vagbo CB, Shi Y, Wang WL, Song SH, Lu Z, Bosmans RP, Dai Q, Hao YJ, Yang X, Zhao WM, Tong WM, Wang XJ, Bogdan F, Furu K, Fu Y, Jia G, Zhao X, Liu J, Krokan HE, Klungland A, Yang YG, He C (2013) ALKBH5 is a mammalian RNA demethylase that impacts RNA metabolism and mouse fertility. Mol Cell **49:** 18-29

Zhong S, Li H, Bodi Z, Button J, Vespa L, Herzog M, Fray RG (2008) MTA is an Arabidopsis messenger RNA adenosine methylase and interacts with a homolog of a sex-specific splicing factor. Plant Cell **20:** 1278-1288

Zhou G, Niu R, Zhou Y, Luo M, Peng Y, Wang H, Wang Z, Xu G (2021) Proximity editing to identify RNAs in phase-separated RNA binding protein condensates. Cell Discov **7:** 72

Zhou L, Tang R, Li X, Tian S, Li B, Qin G (2021) N^6-methyladenosine RNA modification regulates strawberry fruit ripening in an ABA-dependent manner. Genome Biol **22:** 168

Zhou L, Tian S, Qin G (2019) RNA methylomes reveal the m^6A-mediated regulation of DNA demethylase gene SlDML2 in tomato fruit ripening. Genome Biol **20:** 156

Figure legends

Figure 1. PheALKBH9 is involved in abiotic and biotic stress responses.

(A) The evolutionary relationship of the ALKBH family in humans, *Arabidopsis*, *Oryza sativa*, and *Phyllostachys edulis*. *PheALKBH9* was marked with a red asterisk. (B) The gene expression levels of *PheALKBH9* upon drought stress (PEG), salt stress (NaCl), salicylic acid treatment (SA), and abscisic acid (ABA) treatment in Moso bamboo were presented as Transcripts Per Million (TPM). Previously published RNA-seq data comprising three biological replicates were re-analyzed. Data are given as the means ± SD. (*$P < 0.05$, **$P < 0.01$, ***$P < 0.001$, Student's *t*-test, two-tailed). (C) The gene expression levels of *PheALKBH9* in Moso bamboo after BaMV infection. Two biological replicates (n=9) were used in the experiment. Data are given as the means ± SD (*$P < 0.05$, Student's *t*-test, two-tailed). Scale bar = 1cm. (D) Subcellular localization of PheALKBH9 in tobacco epidermal cells. The arrow represents the nuclear localization of the PheALKBH9. Scale bar = 25 μm. (E) Phenotype of *OE-PheALKBH9* grown for 3 weeks (hydroponic culture seedlings) and 2 months (grown in the soil). Scale bar = 10 cm. (F-G) Phenotype F) and statistical analysis G) of grains of OE-*PheALKBH9* (Scale bar = 1cm). Grains from three biological replicates (n=15) were recorded. Data are presented as means ± SD. (Student's *t*-test, two-tailed). WT means wild type kitaake. (H) Blast disease lesions in WT and *OE-PheALKBH9* seedlings. Rice leaves from three biological replicates (n=9) were analyzed. Scale bar = 0.5 cm. (I) The lesion number and fungal biomass was detected on the leaves of WT and *OE-PheALKBH9* by DNA-based qPCR. *OsActin* served as the reference gene. Data are given as the means ± SD for 3 biological replicates (**$P < 0.01$, Student's *t*-test, two-tailed).

Figure 2. The overall impact of *PheALKBH9* overexpression on m^{6}A modification levels in rice.

(A) The Venn diagram shows the number of genes with m^{6}A modification in WT and *OE-PheALKBH9*. WT means wild type kitaake. (B) The number of m^{6}A modification sites in WT and *OE-PheALKBH9*. (C) Percentage of m^{6}A modification sites in CDSs and UTRs. (D) Metagene plot showing the density distribution of m^{6}A sites along the gene body. (E) m^{6}A modification levels in WT and *OE-PheALKBH9*. The box limits represent the 25th and 75th percentiles and the center line represents the 50th percentiles. Whiskers were 1.5× interquartile range extending from the edge of the box. The Mann-Whitney U test was used for statistical test. WT, n=26050, *OE-PheALKBH9,* n=24318. (F) Scatter plot displayed m^{6}A modification ratio. Hyper (pink) and Hypo (blue) methylated m^{6}A modification sites in *OE-PheALKBH9* compared to WT. (G) Dot-blot assay revealed the overall m^{6}A levels in WT and *OE-PheALKBH9*. (H) GO enrichment analysis for hypo-methylated genes. Dot color encodes GO-term enrichment significance (−log10 adjusted p value; blue indicates smaller p values). Dot size represents the number of input genes annotated to the term (Count)

Figure 3. Identification of target RNAs bound by PheALKBH9 in rice and Moso bamboo with HyperTRIBE method.

(A) Schematic diagram of HyperTRIBE method for fused protein PheALKBH9-ADARcd^{E488Q} editing A to I in target RNAs. (B) Schematic diagram of *UBI_{PRO}: PheALKBH9-ADARcd^{E488Q}-FLAG* vector. (C) The percentage of different editing types in WT, *OE-ADAR,* and *OE-PheALKBH9-ADAR*. The bottom panel was editing sites in *OE-PheALKBH9-ADAR* after subtracting the A-G sites detected in WT and ADAR. WT means wild type kitaake. (D) Intersection of A-G editing sites (left panel) and genes (right panel) among line 10, 17, 29 of *OE-PheALKBH9-ADAR*. The 2243 editing sites and 2063 genes were marked in bold blue font. (E) Percentage of A-G editing sites within CDSs and UTRs in three lines. (F) Metagene plot showed the density distribution of A-G editing sites along the 5′ untranslated region (5′UTR), coding sequences (CDSs) and 3′ untranslated regions (3′UTR) in *OE-PheALKBH9-ADAR*. (G) The Percentage of different editing types in the T1 generation of *OE-PheALKBH9-ADAR*. (H) The intersection of A-G editing genes detected in the T1 generation of *OE-PheALKBH9-ADAR*. (I) The intersection of A-G editing genes detected in *OE-PheALKBH9-ADAR* of T1 generation and T0 generation. (J) Intersections of PheALKBH9 target genes and hypo-methylated genes. (K) Schematic diagram illustrating the constructs of *$35S_{PRO}$:ADARcd-Flag* and *$35S_{PRO}$:PheALKBH9-ADARcd-FLAG* vector. (L) Percentage distribution of different editing types observed in bamboo protoplasts overexpressing PUC22 (EV), *ADAR,* or *$35S_{PRO}$:PheALKBH9-ADARcd-FLAG*. (M) Venn diagram illustrating the overlap of PheALKBH9-target genes between Moso bamboo and rice (left panel). Right panel shows the overlap 134 conserved target genes (between bamboo and rice) and 2594 genes containing hypo-methylated sites. The upper part showed that *PABPC1* and *PABPC2* were bound by ALKBH9 based on HyperTRIBE data. (N) Bar chart illustrating the m^6A modification levels of *PABPC1* and *PABPC2* in WT and *OE-PheALKBH9*.

Figure 4. Analysis of the correlation between m^{6}A modification changes and protein alterations induced by *PheALKBH9*.

(A) Volcano plot shows differentially expressed proteins (DEPs), with significantly upregulated and downregulated protein levels represented in pink and blue, respectively. (B) Heatmap of DEPs. The color scale bar displays row-wise z-scores (centered at 0); darker blue indicates higher expression, while lighter blue indicates lower expression. (C) KEGG analysis of DEPs. (D) The bar graph depicts the fold change in transcriptional and protein levels of genes in *OE-PheALKBH9* compared to WT with 2 different transgenic lines. WT means wild type kitaake. (E-F) Negative correlation between m^{6}A modification level and protein expression in WT (E) and *OE-PheALKBH9* (F). Pearson's R is reported; the p value was determined by two-sided Student's t test. (G-J) Venn diagrams show the intersection of DEPs with hypermethylated genes (G, H) and hypomethylated genes (I, J).

Figure 5. Influence of *PheALKBH9* on transcript poly(A) tails in rice.

(A) Distribution plot of PAL (poly(A) tail length) in WT and *OE-PheALKBH9* based on nanopore DRS. (B) Volcano plot showed genes with differential changes on PAL, with *OsCAF1G* marked by a red dot. WT means wild type kitaake. (C) GO enrichment analysis of genes with significantly shortened PAL. Dot color encodes GO-term enrichment significance (−log10 adjusted p value; blue indicates smaller p values). Dot size represents the number of input genes annotated to the term (Count). (D-E) Correlations between PAL (poly(A) tail length) and protein expression (D) and between PAL and m^6A modification level (E). Solid line shows the ordinary least squares (OLS) fit. Pearson's r is reported; p values were obtained using a two-sided Student's t test. (F) A boxplot illustrating the fold changes in m^6A levels of genes categorized into differential and non-differential PAL groups following overexpression of PheALKBH9. Boxes indicate the 25th–75th percentiles (IQR) with the median as the center line; whiskers extend to 1.5×IQR from the box. Statistical comparisons were performed using two-sided Mann–Whitney U tests. (G) Overlap of shortened PAL genes and hypo-methylated genes. (H) Three bar chart illustrating the result of *OsCAF1G* in WT and *OE-PheALKBH9* for m^6A ratio (left panel), PAL (middle panel) and m^6A - IP - qPCR (right panel). In the m^6A - IP - qPCR assay, data are given as the means ± SD from three independent biological replicates (*$P < 0.05$, **$P < 0.01$, ***$P < 0.001$, Student's *t*-test, two-tailed).

Figure 6. Dual-Luciferase Assay demonstrated that the m^{6}A site of *Perox4* affected firefly luciferase activity.

(A) Heatmap illustrating the gene expression of 13 genes in WT and Guy11 innovated rice. The color scale bar displays row-wise z-scores (centered at 0); darker blue indicates higher expression, while lighter blue indicates lower expression. WT means wild type kitaake. (B) RT-qPCR results confirmed the upregulation of gene related to plant immune response. Data are given as the means ± SD from three independent biological replicates (*P < 0.05, **P < 0.01, ***P < 0.001, Student's t-test, two-tailed). (C) Bar chart illustrating the m^{6}A ratio, expression level, protein level, and m^{6}A-IP-qPCR validation of *OsPerox4*. Data are given as the means ± SD from three independent biological replicates (*P < 0.05, **P < 0.01, ***P < 0.001, Student's t-test, two-tailed). Gene expression was presented as Transcripts Per Million (TPM). The browser view showed the expression and m^{6}A modification of *Perox4* in WT and *OE-PheALKBH9*. The bottom part of the diagram was gene structure of *Perox4*. (D) Prediction of the interaction between PheALKBH9 and 100 bp RNA sequence surrounding the m^{6}A modification site of *Perox4* using AlphaFold3. (E) Schematic diagram of the WT and mutant plasmid. (F) Detection of Firefly luciferase activity in tobacco leaf. The color scale bar on the right indicates the intensity of firefly luciferase, with gradient colors ranging from low to high. Scale bar = 1cm. (G) Quantification of Firefly luciferase activity using a luciferase assay system. Three biological replicates (n=9) were used in the experiment. Data are given as the means ± SD (*P < 0.05, **P < 0.01, ***P < 0.001, Student's t-test, two-tailed). (H) Regulatory model illustrating the role of PheALKBH9 in rice response to blast fungal. PheALKBH9 binds to genes involved in blast response, such as *Perox4*, *OsJAZ7* and *OSMETS2,* leading to reduced m^{6}A modification and potentially influencing their expression, thereby affecting blast resistance.

Figure 1

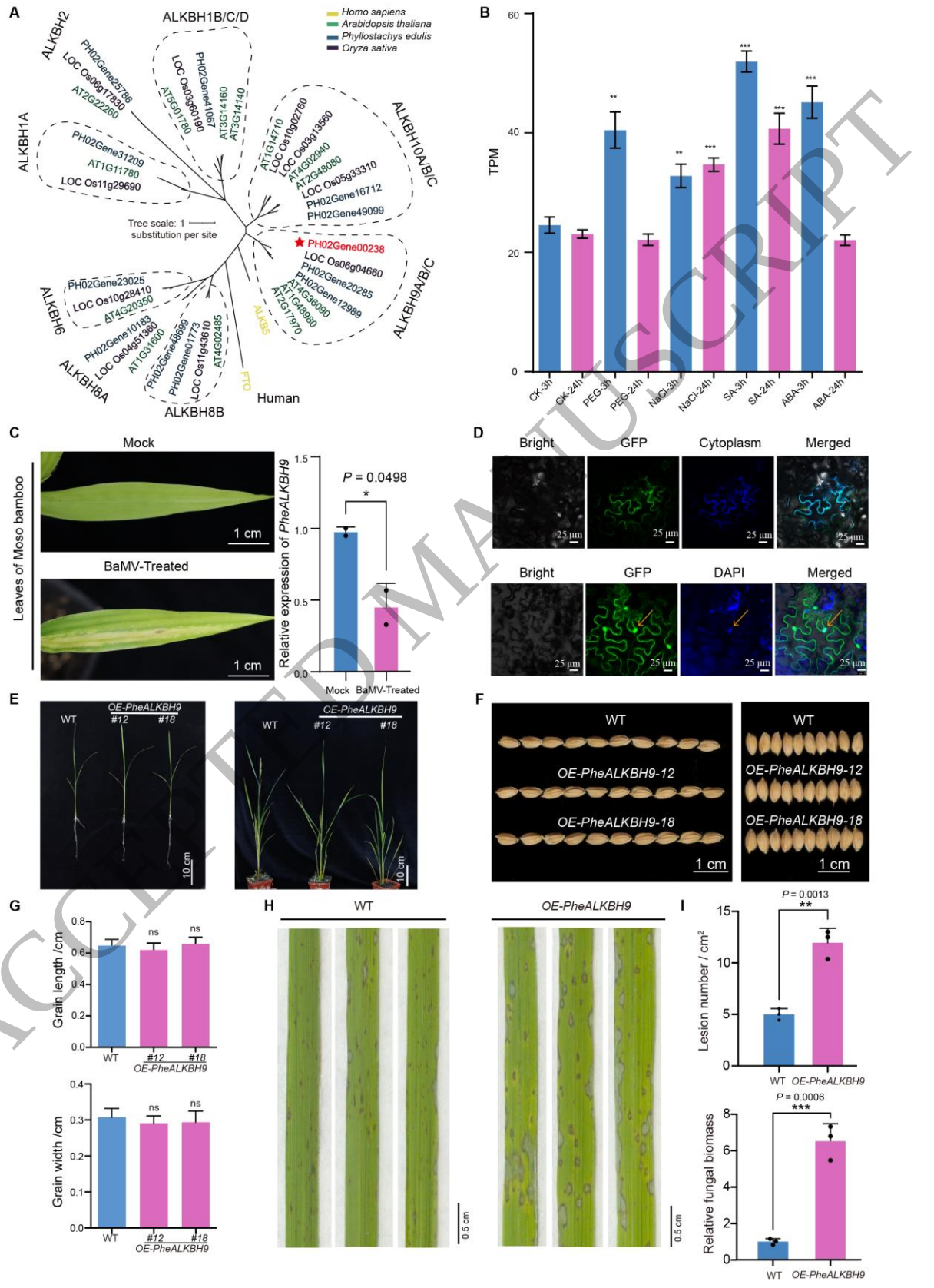

Figure 2

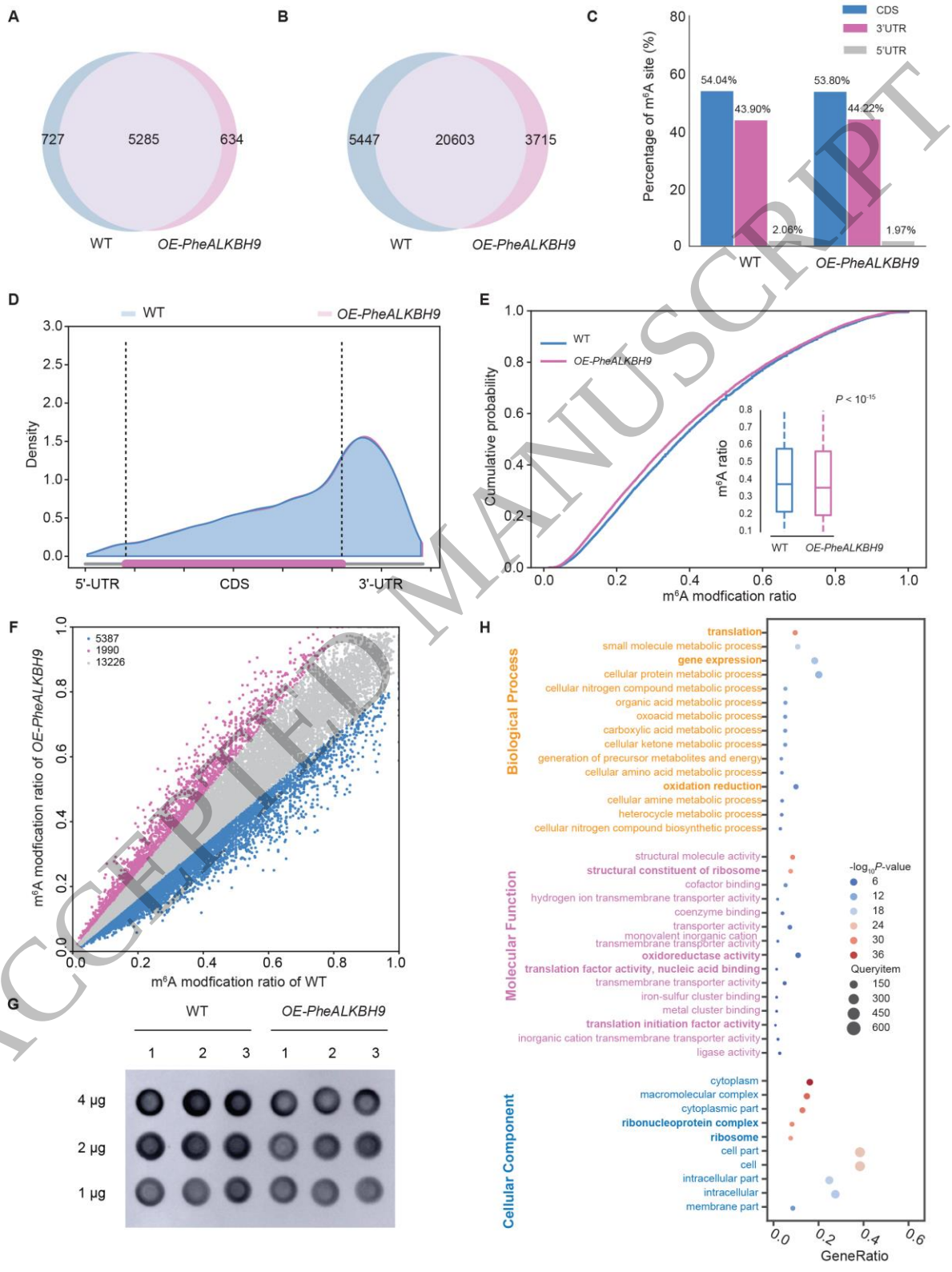

1

Figure 3

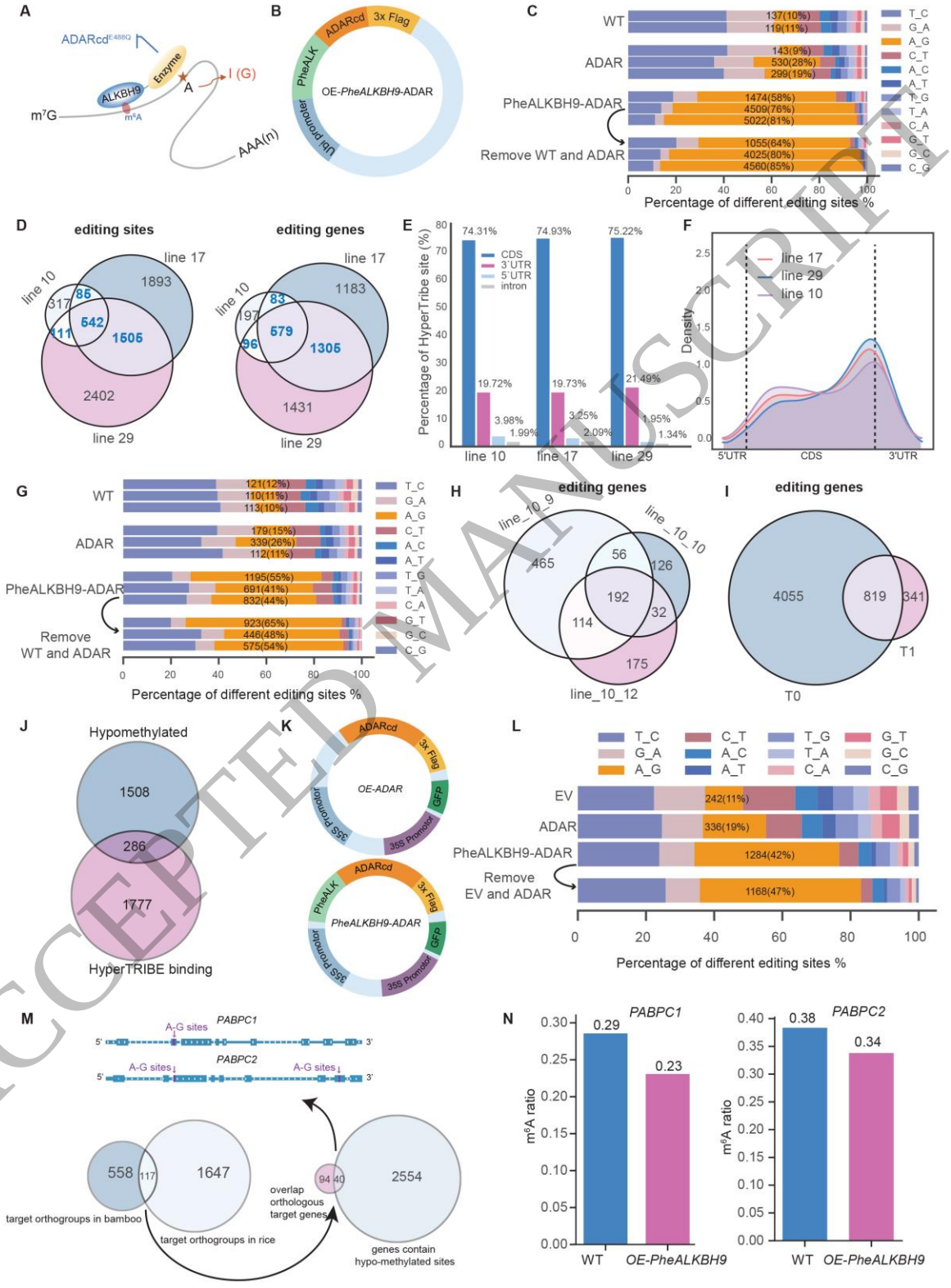

1

Figure 4

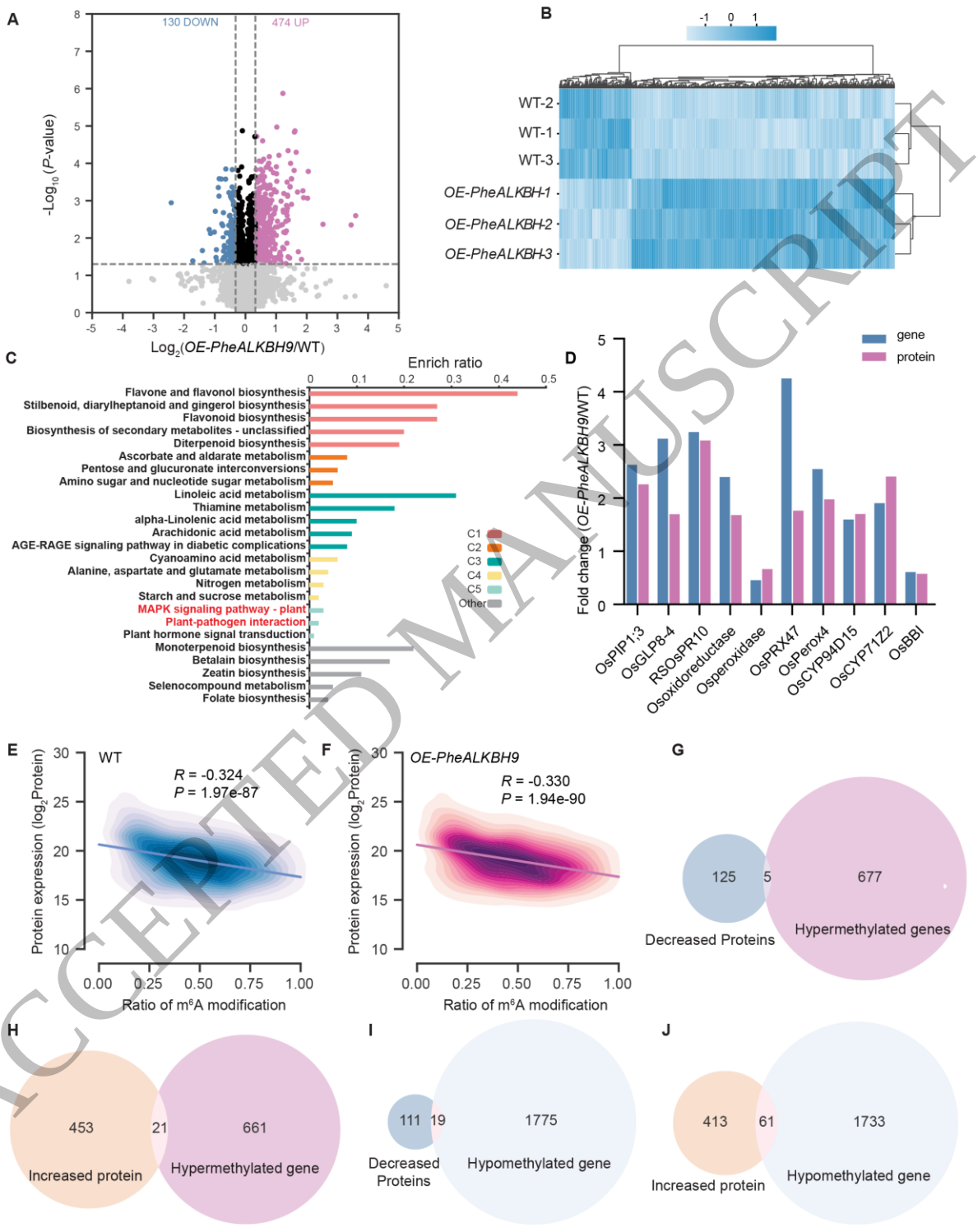

Figure 5

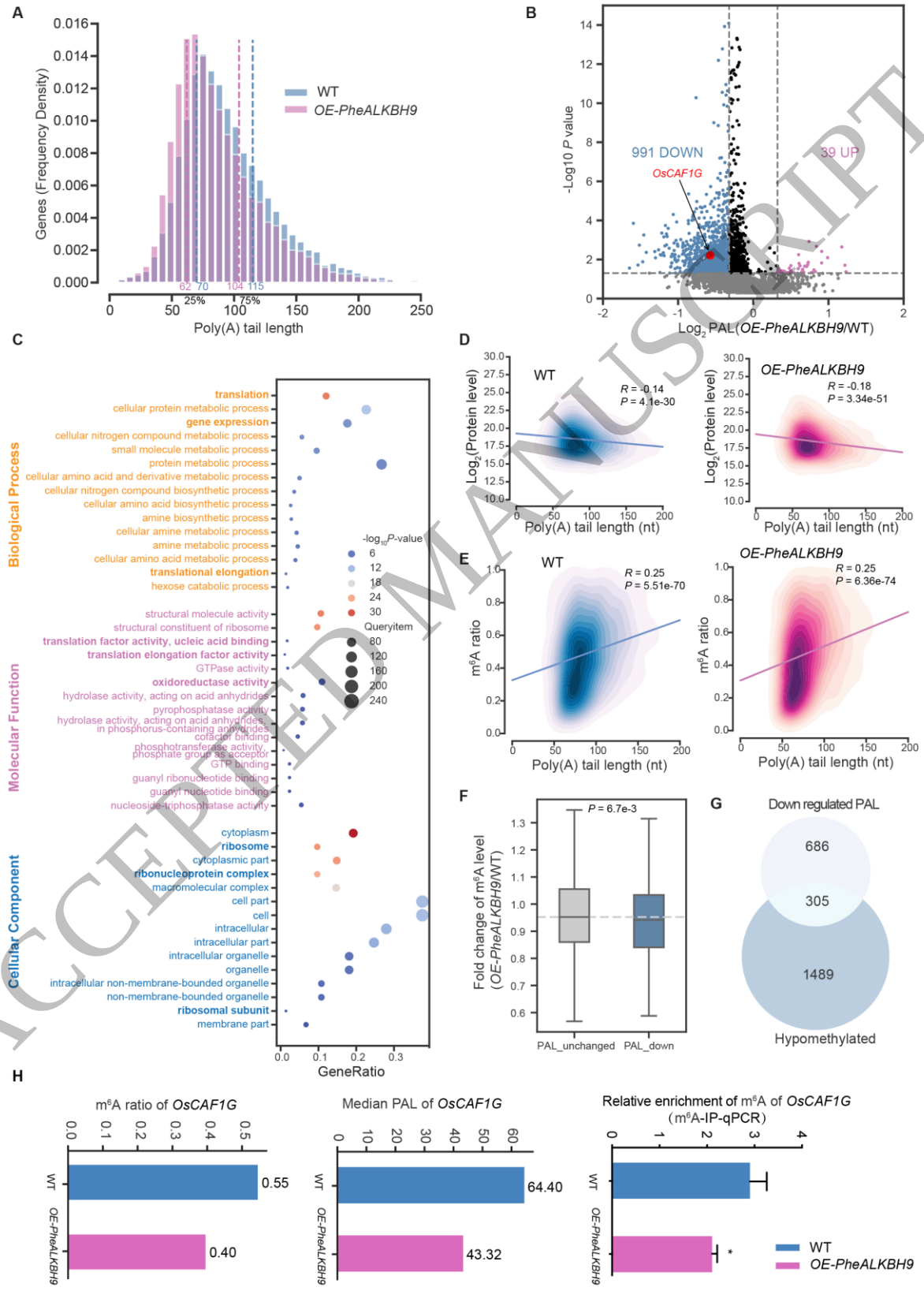

Figure 6